This is the accepted manuscript of the article, which has been published in Journal of Cell Science. 2020, 133(9). http://dx.doi.org/10.1242/jcs.242404

Induction of ligand promiscuity of αVβ3 integrin by mechanical force

Michael Bachmann[1,2,*], Markus Schäfer[1,3,*], Vasyl V. Mykuliak[4], Marta Ripamonti[2], Lia Heiser[1], Kai Weißenbruch[1], Sarah Krübel[1], Clemens M. Franz[5,6], Vesa P. Hytönen[4], Bernhard Wehrle-Haller[2,7], Martin Bastmeyer[1,3,7]

Affiliations:

1: Zoological Institute, Cell- and Neurobiology, Karlsruhe Institute of Technology (KIT), Karlsruhe, Germany

2: Department of Cell Physiology and Metabolism, University of Geneva, Geneva, Switzerland

3: Institute of Functional Interfaces (IFG), Karlsruhe Institute of Technology (KIT), Karlsruhe, Germany

4: Faculty of Medicine and Health Technology and BioMediTech, Tampere University, Tampere, Finland and Fimlab Laboratories, Tampere, Finland

5: DFG–Center for Functional Nanostructures, Karlsruhe Institute of Technology (KIT), Karlsruhe, Germany

6: WPI Nano Life Science Institute, Kanazawa University, Kanazawa, Japan

7: Correspondence should be addressed to B. Wehrle-Haller (bernhard.wehrle-haller@unige.ch) or M. Bastmeyer (martin.bastmeyer@kit.edu).

*: These authors contributed equally.

Key words:

αVβ3 integrin, ECM, ligand selection, focal adhesions, fibronectin, mechanosensing

Summary statement (15-30 words):

Most integrins can bind several ligands. This work demonstrates how one integrin, αVβ3, selects between two different ligands, fibronectin and vitronectin, based on force-regulated conformational changes in αVβ3 integrin.

Abstract:

αVβ3 integrin can bind to multiple extracellular matrix proteins, including vitronectin (Vn) and fibronectin (Fn), which are often presented to cells in culture as homogenous substrates. However, in tissues, cells experience highly complex and changing environments. To better understand integrin ligand selection in such complex environments, we employed binary-choice substrates of Fn and Vn to dissect αVβ3 integrin-mediated binding to different ligands on the subcellular scale. Super-resolution imaging revealed that αVβ3 integrin preferred binding to Vn under various conditions. In contrast, binding to Fn required higher mechanical load on αVβ3 integrin. Integrin mutations, structural analysis,

and chemical inhibition experiments indicated that the degree of hybrid domain swing-out is relevant for the selection between Fn and Vn; only a force-mediated, full hybrid domain swing-out facilitated αVβ3-Fn binding. Thus, force-dependent conformational changes in αVβ3 integrin increased the diversity of available ligands for binding and therefore enhanced the ligand promiscuity of this integrin.

List of abbreviations:

Fbg, fibrinogen; Fn, fibronectin; FnIII10, 10th domain of fibronectin; MEF, mouse embryonic fibroblast; MEF vcl -/-, mouse embryonic fibroblasts derived from vinculin knockout mice; MD, molecular dynamics; NMIIA, nonmuscle myosin IIA; Opn, osteopontin; Tsp, thrombospondin; Vn, vitronectin;

Introduction:

Integrins are important cell adhesion receptors and consist of α- and β-subunits forming transmembrane heterodimers (Bachmann, Kukkurainen, Hytönen, & Wehrle-Haller, 2019; Campbell & Humphries, 2011). In their active state, the extracellular part binds to proteins of the extracellular matrix (ECM) or proteins on other cells, while the intracellular part is connected to actin via multiple adapter and signaling proteins that make up the so-called adhesome (Byron, Humphries, Bass, Knight, & Humphries, 2011; Hytönen & Wehrle-Haller, 2014; Kuo, Han, Hsiao, Yates, & Waterman, 2011; Schiller et al., 2013). Activating integrins requires conformational changes that include extension of the extracellular domains and opening of the integrin headpiece. The respective steps in activation are named bent-closed, extended-closed, and finally extended-open conformation. In β-integrin subunits, headpiece opening is characterized by the swing-out of the hybrid domain from the βI-like domain (Eng, Smagghe, Walz, & Springer, 2011; Zhu & Springer, 2013). Molecular dynamics (MD) simulations indicated that force supports this hybrid domain swing-out and thereby leads to full integrin activation (Puklin-Faucher, Gao, Schulten, & Vogel, 2006; Zhu et al., 2008). The best studied cases of force-dependent ligand-integrin interactions are the binding of αVβ3 and α5β1 integrin to fibronectin (Fn) (Engler, Chan, Boettiger, & Schwarzbauer, 2009; Fernandez-Sauze, Grall, Cseh, & Van Obberghen-Schilling, 2009; Takahashi et al., 2007; van der Flier et al., 2010). Considerable effort has been invested to understand individual and cooperative effects of this αVβ3/Fn- and α5β1/Fn-binding (Benito-Jardón et al., 2017; Roca-Cusachs, Gauthier, Del Rio, & Sheetz, 2009; Schiller et al., 2013; White, Caswell, & Norman, 2007). At the same time, however, it is less clear how an individual integrin can discriminate between different ligands. Work with the RGD peptide (ligand binding site for αVβ3 and α5β1 among several other integrins) has indicated that conformational changes around the RGD sequence (cyclic vs. linear peptide) can cause integrin selectivity (Mas-Moruno, Rechenmacher, & Kessler, 2010; Pierschbacher & Ruoslahti, 1987). But whether these findings have a relevance for physiological ligands remained to be tested. At the same time, more than 12 potential RGD-ligands for αVβ3 integrin have been reported (Humphries, Byron, & Humphries, 2006) but it remains unclear whether or how these ligands are selected by αVβ3 integrin. We have recently developed a method to produce microstructured fibronectin/vitronectin (Fn/Vn) substrates to analyze ligand selection by αVβ3 integrin on a cellular level (Pinon et al., 2014; Rahikainen et al., 2017; Soto-Ribeiro et al., 2019). Fn is a structural component of the ECM and has essential functions during development (George,

Georges-Labouesse, Patel-King, Rayburn, & Hynes, 1993). Vn, on the other side, is a matrisomal protein with no relevant structural role for the ECM, while regulating inflammation and wound healing in healthy and in cancer settings (Gladson, Wilcox, Sanders, Gillespie, & Cheresh, 1995; Keasey et al., 2018; Preissner & Reuning, 2011). Interestingly, both Fn and Vn are present at high concentrations in the blood (Fn: 300 µg/ml (Pankov & Yamada, 2002); Vn: 200-400 µg/ml (Preissner & Reuning, 2011)) suggesting a need for fibroblasts to select between these different ECM proteins after wounding.

Here we combined Fn/Vn substrates with super-resolution microscopy and super-resolution live cell imaging. We analyzed the interaction of αVβ3 integrin with different ligands by using αVβ3 integrin mutants and pharmacological inhibitors. We found a clear preference of αVβ3 integrin for Vn under a wide range of conditions. Surprisingly, we revealed that mechanical load on αVβ3 integrin enabled Fn binding while Vn is already recognized by αVβ3 integrin under lower mechanical load. Additional experiments indicated that this selection of ligands is coupled to force-regulated integrin conformations. Under low force conditions, or when mutationally prevented from full headpiece opening, αVβ3 integrin binds only to Vn. On the other side, mechanical pull induces a full hybrid domain swing-out to the extended-open conformation (Puklin-Faucher et al., 2006; Zhu et al., 2008). In this conformation αVβ3 integrin gains the ability to bind to Fn indicating a more promiscuous integrin-ligand relationship. We further show that these ligand-binding properties modulate cellular behavior during spreading, migration, and mechanotransduction depending on the respective ECM protein. Finally, we established additional ligand combinations and found that osteopontin (Opn) phenocopied Vn in binary choice substrates while fibrinogen (Fbg) resembled Fn. This indicates that the mechanism of differential ligand selectivity of αVβ3 integrin can be transferred to a wider range of integrin-ligand combinations.

Results:

Vitronectin is the preferred ligand for αVβ3 integrin

To study how the simultaneous presentation of two ECM ligands influences binding choice of αVβ3 integrin, we produced Fn/Vn substrates with subcellular resolution (Pinon et al., 2014). 2x2 µm squares of Fn separated by 1 µm gaps were stamped onto a coverslip and the remaining surface was covered with Vn, leading to a clear separation of both proteins with a geometrical coverage of equal contribution (Pinon et al., 2014). The quality of substrates was analyzed by fluorescence and atomic force microscopy (Fig. 1A, B). To specifically analyze GFP tagged β3-integrin without competition by endogenous αVβ3 integrin we used a subclone of NIH3T3-cells expressing low levels of endogenous β3-integrin (Fig. S1A and (Pinon et al., 2014)). Furthermore, in these cells αV-integrin is the only subunit pairing with β3-integrin. Thus, our results with β3-integrin are synonymous for αVβ3-integrin. To study the binding choice of αVβ3-integrin on Fn/Vn substrates, cells were transfected with GFP tagged β3-wt integrin, cultured for 2 hrs, and immunolabeled. Paxillin was used as a marker to detect all integrin-mediated adhesions. Super resolution structured illumination microscopy (SR-SIM) revealed paxillin clusters on both Fn and Vn coated areas. In contrast, αVβ3 integrin revealed a strong

preference to Vn (83.5% colocalization; Fig 1C, D). This preference was not dependent on the size of αVβ3 integrin mediated adhesions (Fig. 1F). To exclude that the low amount of αVβ3 integrin on Fn is caused by competition and steric hindrance with endogenous α5β1 integrin, we tested β1 integrin deficient GD25 cells on Fn/Vn substrates. We observed the same preference of αVβ3 integrin for Vn (82.8%; Fig. S1D, F). Furthermore, this preference for Vn was reproducible for a wide range of experimental conditions such as pattern geometry and stamping order (Fig. S1G, I), the ratio of Fn/Vn used to prepare Fn/Vn substrates (Fig. S1B), or substrate stiffness (Fig. S1J-L). Substrates homogenously coated with either Fn or Vn also supported these findings: Both area and intensity of αVβ3 integrin adhesions are significantly increased on Vn as compared to Fn (Fig S2).
Next, we measured the interaction of αVβ3 integrin with Fn and Vn *in vitro* using biolayer interferometry (Fig. 1E). Whereas Fn dissociated rapidly from αVβ3 integrin, Vn-binding to αVβ3 was non-dissociable. Work by Orlando and Cheresh also observed a non-dissociable binding between Vn and αVβ3 (Orlando & Cheresh, 1991), however contrasting with work by Chillakuri and colleagues (Chillakuri, Jones, & Mardon, 2010). To test our findings in light of these contradicting observations we analyzed Vn-αVβ3 integrin interaction in presence of the RGD mimetic αVβ3 integrin inhibitor cilengitide (Fig. S3E). The dissociation of Vn from αVβ3 integrin in presence of cilengitide confirmed that we observed a specific, RGD-dependent interaction between Vn and αVβ3 integrin (Fig. 1E). This corroborates our finding of a non-dissociable, RGD-dependent interaction between αVβ3 integrin and Vn in this *in vitro* assay. However, such a difference in binding behavior might also imply that αVβ3 integrin binding to Fn is unlikely whenever Vn is present. In contrast, on Fn/Vn substrates, we observed a colocalization of αVβ3 integrin with Fn of 16.5% (Fig. 1C, D). To understand the binding of αVβ3 integrin to Fn in a cellular context we studied the dynamics of αVβ3 integrin mediated adhesion formation in living cells. First, we performed atomic force microscopy (AFM)-based single-cell force spectroscopy (Dao et al., 2012; Langhe et al., 2016). β1-deficient GD25 cells were attached to the AFM cantilever and alternatingly brought in contact with homogenously coated Fn and Vn areas. Detachment forces during cell retraction were measured after 10s, 30s, and 120s of contact. After 30s and 120s of adhesion, significantly higher forces were needed to detach cells from Vn as compared to Fn (Fig 1G) indicating that αVβ3 integrin mediated adhesions formed and/or matured faster on Vn.
Next, we observed β3-wt GFP expressing NIH3T3 cells on Fn/Vn substrates using SR-SIM live cell imaging. During spreading cells initiated numerous nascent adhesions on these binary choice substrates (Fig. 1H and Video S1 and S2). These αVβ3 integrin mediated adhesions almost exclusively formed on Vn (Fig. 1I), while during adhesion maturation some adhesions were translocated onto Fn in a centripetal direction towards the cell center and in direction of retrograde actin flow (yellow arrows in Fig. 1H and Video S2). Thus, observed in vitro and in a cellular context, αVβ3 integrin prefers binding to vitronectin over fibronectin. Interestingly, live cell imaging indicated that actin flow - and therefore mechanical forces - might be an important parameter involved in the binding of Fn by αVβ3 integrin.

Actomyosin contractility regulates the ligand preference of αVβ3 integrin

To test whether intracellular forces are involved in the binding choice of αVβ3 integrin, we reduced actomyosin contractility with blebbistatin or Y27632. Blebbistatin inhibits myosin directly while

Y27632 inhibits the Rho/ROCK pathway and thereby reduces myosin activity. Both inhibitors increased the number of small, round nascent adhesions in the cell periphery (Fig. 2A, B) and additionally caused a significant decrease in colocalization of β3-wt GFP integrin with Fn (Fig. 2G and Fig. S3A; ≈ 2.5-fold decrease). Incubating cells for 6 hrs in the presence of blebbistatin caused no improvement in Fn localization of αVβ3 integrin, indicating that reduced contractility does not delay but rather prevents Fn binding by αVβ3 integrin (Fig. S1C, H). Vinculin is well established as an important part of the molecular clutch to transmit forces from actin to the integrin-ECM bond (Humphries et al., 2007; Rahikainen et al., 2017; Thievessen et al., 2013). Therefore, we analyzed the localization of β3-wt GFP integrin on Fn/Vn substrates in mouse embryonic fibroblasts derived from vinculin knockout mice (MEF Vcl -/-). Indeed, the absence of vinculin caused a decrease in Fn binding of αVβ3 GFP integrin (Fig. 2E, H), which was comparable to blebbistatin or Y27632 treatment (Fig. 2G). In contrast, re-expression of vinculin mCherry in MEF Vcl -/- cells increased the Fn localization of αVβ3 GFP integrin to control-levels (Fig 2 D,F,H). To enhance the mechanical load on integrins, we overexpressed non-muscle myosin IIA mApple (NMIIA) in NIH3T3 cells (Fig. 2C). Additional NMIIA caused an increase of αVβ3 GFP integrin localization on Fn (Fig. 2G; ≈ 1.5-fold increase). Taken together, these findings indicate that αVβ3 integrin binding to Fn is fostered by intracellular force and vinculin, whereas Vn is recognized by αVβ3 integrins already under low mechanical load.

Hybrid domain swing-out is required for Fn binding of αVβ3 integrin

Next, we asked whether enhanced activation of αVβ3 integrin could substitute mechanical forces during Fn binding. Therefore, we employed either Mn^{2+} activation of αVβ3 integrin (Fig. 3A), or established mutations to activate integrins (Fig. 3B-D): (i) Mn^{2+} treatment increases the affinity of the integrin headpiece for the ligand (Zhu & Springer, 2013), (ii) the β3-VE mutation has a 20-fold higher affinity for talin (Pinon et al., 2014), (iii) the β3-D723A mutation disrupts the inhibitory salt-bridge at the inner membrane clasp between the αV- and β3-subunits (Saltel et al., 2009), and (iv) β3-N305T has been reported to cause a constitutive hybrid domain swing-out and slower integrin dynamics (Cluzel et al., 2005; Luo, Springer, & Takagi, 2003). Surprisingly, on Fn/Vn substrates, only β3-N305T showed a significant increase of colocalization with Fn (Fig. 3F; ≈ 1.5-fold increase), whereas Mn^{2+} treatment and the intracellular activating mutations (β3-VE and β3-D723A) caused no significant difference. However, Vn remained the preferred ligand for all conditions. Importantly, endogenous αVβ3 integrin is basically absent in the NIH3T3 cells we used (Fig. S1A) and therefore does not compete with β3 mutations used in this experiment. Next, we used SR-SIM live cell imaging to test whether the conformational changes caused by the β3-N305T mutation are accompanied by the ability to initiate adhesions on Fn (Fig. 3J and Video S3, S4). We observed that spreading cells initiated most β3-N305T-mediated adhesions on Vn but in contrast to β3-wt integrin few adhesions initiated on Fn as well (Fig. 3K). The mutation β3-VE caused a non-significant but observable increase in Fn colocalization (Fig. 3F). However, β3-VE failed to initiate adhesions on Fn similar to β3-wt (Fig. 3K and Video S5, S6) again highlighting the relevance of the head-piece opening, rather than talin-mediated β3-integrin activation, for Fn binding.

Interestingly, all activating conditions caused central clusters of αVβ3 integrin with irregular shapes compared to peripheral adhesions (Fig. 3A-D, zoom-in 2). Similar integrin clusters have been

reported to appear within minutes after Mn^{2+} addition (Cluzel et al., 2005; Saltel et al., 2009). On Fn/Vn substrates, these clusters were almost exclusively localized on Vn (Fig. S3F). Analysis of several integrin adapter proteins demonstrated talin recruitment but no association of paxillin, vinculin, or actin stress fibers to these αVβ3 integrin clusters (Fig. 3A-D, Fig. S3G-I). This suggests that they are not mechanically coupled to the actin cytoskeleton and thus are under low mechanical load (compare to MEF Vcl -/- cells; Fig. 2E, H). The exclusive localization of these 'low-force adhesions' on Vn confirms our observations using contractility inhibitors and vinculin -/- cells and emphasizes the requirement of mechanical load on αVβ3 integrin to bind to Fn in contrast to Vn.

In summary, our experiments showed that only αVβ3 integrin activation by the N305T mutation increases Fn localization of αVβ3 mediated focal adhesions. Furthermore, β3-N305T allows the initiation of adhesions on Fn in contrast to other β3 integrin activating conditions. This indicates that hybrid-domain swing-out is a crucial step for the ability of aVb3 integrin to bind to Fn.

Complete force-dependent hybrid domain swing-out is necessary for Fn binding

The unique ability of β3-N305T to increase Fn binding (Fig. 3F) motivated us to study this mutation in more detail. The creation of a glycosylation site between the βI-like and the hybrid domain at Asn 303 (N303) is proposed to cause a constitutive hybrid domain swing-out and thereby full integrin activation. To experimentally dissect the steric effect of N303-glycosylation from force-induced hybrid domain swing-out (Puklin-Faucher et al., 2006; Zhu et al., 2008), we treated β3-N305T expressing cells with blebbistatin (Fig. 3E). β3-N305T mediated adhesions appeared less affected by blebbistatin as compared to b3-wt (compare to Fig. 2A; 10 µM blebbistatin in both experiments). Whereas β3-wt only formed nascent adhesions, β3-N305T showed both nascent adhesions and partially matured, elongated adhesions. However, the colocalization of β3-N305T GFP with Fn was clearly reduced in the case of reduced cellular contractility (Fig. 3G; ≈ 5-fold decrease). This indicates that the conformational change induced by the glycan wedge alone may not be sufficient to increase Fn-binding in the absence of mechanical forces on αVβ3 integrin. We observed the same effect of reduced Fn-binding for all other activating conditions when combined with a blebbistatin treatment (Fig. S3B). Thus, all integrin activating conditions relied on mechanical forces for Fn binding of αVβ3 integrin. Even constitutive hybrid domain swing-out as reported for the β3-N305T mutation was not sufficient for efficient Fn binding in conditions of reduced cellular contractility. Apparently, mechanical forces caused additional conformational changes needed for Fn binding.

To understand the impact of force and glycosylation on αVβ3 integrin conformation we employed molecular dynamics (MD) simulations for a αVβ3 integrin structure that was glycosylated at N303. Zhu and colleagues published headpiece opening of αIIbβ3 integrin in eight steps (Zhu & Springer, 2013). We used a Fn-bound structure of αVβ3 integrin (PDB: 4MMX) and arranged a hybrid domain swing-out by superimposition with step seven (PDB: 3ZE1; chain B) in the activation cascade of αIIbβ3 described by Zhu and colleagues. This structure was modified by adding a glycosylation at N303 and equilibrated for 100 ns. The same structure without glycosylation at N303 was used as a control. MD simulations showed that hybrid domains swang out to a similar angle, while the glycosylated form appeared more stable (Fig. 3H, I). Accordingly, glycosylation at N303 might stabilize αVβ3 integrin in a conformation close to full activation. However, the final activation step (step 8

(Zhu & Springer, 2013), PBD: 3ZE2, chain C, D), is characterized by an even further increase in the hybrid domain swing-out ("Fully activated 1" in Fig. 3L). Another published structure of the fully open β3 integrin headpiece (PBD: 3FCU, αIIbβ3) showed a similar maximal hybrid domain swing-out ("Fully activated 2" in Fig. 3L). Thus, comparison of glycosylated and fully activated structures suggested that N303 glycosylation alone is not sufficient to induce the full hybrid domain swing-out. Combining β3-N305T with Mn^{2+} showed no additive effect on Fn-binding (Fig. 3G) as it was the case for adding Mn^{2+} to β3-wt (Fig. 3F).

We conclude that our MD simulations, performed without mechanical pull on the β3-integrin, reflected the structure of β3-N305T integrin in experiments with contractility inhibition (Fig 3E, G). We propose that αVβ3 integrin needs mechanical load for its final activation with maximal hybrid domain swing-out. Only this αVβ3 integrin conformation seems to be able to stably bind Fn in a cellular environment.

Extended-open conformation of αVβ3 integrin is not necessary for Vn binding

Our experiments indicated that stable Fn-binding by αVβ3 integrin requires force-dependent hybrid domain swing-out. In contrast, αVβ3 integrin was able to bind Vn in experiments where cell contractility was reduced. Accordingly, we wanted to test whether αVβ3 integrin can bind Vn already in the extended-closed conformation. To this end, we set out to develop an integrin mutation locking αVβ3 integrin in the extended-closed conformation. We created a disulfide bridge between the βI-like and the hybrid domain of β3 integrin to limit the degree of the hybrid domain swing-out (β3-V80C/D241C). Structural analysis supported our rationale for this mutation (Fig. 4A). We prepared a model, where cysteine mutations were introduced into extended-closed conformation of αVβ3 integrin (PDB: 4MMX) using PyMOL and energy minimization of the model. The disulfide bridge caused only minimal distortion of the protein; the distance between Cα atoms of V80C and D241C after introducing a disulfide bond did not change compared to the wildtype situation (both structures: d = 6.3 Å). In contrast, αVβ3 integrin in the extended-open conformation showed an increased distance by a factor of three (d = 19.4 Å) between Cα atoms of V80 and D241, implying that a V80C-D241C disulfide bridge can block the transition to the extended-open conformation.

Next, we expressed β3-V80C/D241C GFP in NIH3T3 cells and cultured them on substrates homogenously coated with either Fn or Vn (Fig. 4B, C). On both substrates we observed a high GFP background signal potentially indicating that large amounts of β3-V80C/D241C cannot be recruited into adhesion sites. However, the GFP signal revealed a clustering of β3-V80C/D241C into adhesions on Vn but not at all on Fn. Treatment of cells with Mn^{2+} increased the clustering of β3 V80C/D241C into adhesions on Vn but not on Fn (Fig. 4D, E). Adding 1 mM DTT to open disulfid bridges allowed clustering of β3 V80C/D241C on Fn (Fig. S4A, B, E) indicating that the V80C/D241C disulfide bridge formed and that the conformation of β3-V80C-D241C prevents Fn binding. On Fn/Vn substrates we observed weak β3-V80C/D241C GFP positive adhesions that could not be reliably quantified due to the high background signal. However, a restricted localization of β3-V80C/D241C GFP on Vn was obvious (Fig. 4F). Since Mn^{2+} treatment enhanced the recruitment of β3-V80C/D241C into adhesion sites only on Vn (Fig. 4D, E), ligand selection seems not to be influenced by Mn^{2+} (as also observed before; Fig. 3F). Thus, we treated β3-V80C/D241C GFP expressing cells on Fn/Vn substrates with

Mn^{2+}. We observed an enhanced clustering of β3-V80C/D241C GFP into adhesions while still preserving the restriction to Vn (Fig. 4G, H). This increased fluorescence signal allowed a reliable quantification and revealed a significantly reduced localization of β3-V80C/D241C on Fn (8.4% colocalization with Fn; optical sectioning microscopy) as compared to β3-wt integrin (21.8 % colocalization with Fn; optical sectioning microscopy). We analyzed β3-V80C/D241C and β3-wt expressing cells on Fn/Vn substrates also in the presence of 1 mM DTT (Fig. S4C, D, F) and observed increased Fn localization of β3-V80C/D241C treated with DTT. In contrast, β3-wt showed no change in Fn localization due to DTT treatment (β3-wt: 21.8%, β3-wt + 1 mM DTT: 22.3%; β3-V80C/D241C + 1 mM $MnCl_2$: 8.4%; β3-V80C/D241C + 1 mM DTT: 15.8%). A flow cytometry-based assay to measure β3 integrin activation (Pinon et al., 2014) confirmed these observations (Fig. S4G). Importantly, another disulfide bridge mutation locking the integrin in the inactive bent state (β3-V332C/S674C, (Takagi, Petre, Walz, & Springer, 2002)), showed significantly reduced β3 integrin activation in this assay. This supported our rationale that mutationally introduced disulfide bridges form and that they are stable in cell experiments indicating that β3-V80C/D241C is indeed locked in a conformation as presented in figure 4A.

We further extended these data using the integrin inactivator Ca^{2+} (Fig. S3C, D). Treatment of β3-wt GFP expressing cells with Ca^{2+} reduced Fn binding to a similar extent as inhibition of contractility or the β3-V80C/D241C mutation. We also compared the fluorescence recovery after photobleaching (FRAP) of β3-wt, β3-N305T, and β3-V80C/D241C, in order to understand the influence of these mutations on αVβ3 integrin turnover in adhesions (Fig. 4I, Fig. S4H). Interestingly, β3-V80C/D241C GFP showed a very fast turnover compared to β3-wt GFP, while the turnover of β3-N305T GFP was slower than β3-wt GFP, confirming observations in B16F1 melanoma cells (Cluzel et al., 2005). In summary, we propose that αVβ3 integrin is not relying on the fully extended-open conformation to bind Vn, whereas Fn binding needs a conformational change to the extended-open conformation.

Preference for Vn influences cell migration and mechanotransduction

Our results so far revealed a mechanism enabling αVβ3 integrin to differentiate between Fn and Vn based on the degree of the force-dependent hybrid domain swing-out. However, stable binding to any ligand might result in the fully active extended-open conformation of αVβ3 integrin irrespective of the actual ligand present. Therefore, it is possible that the preference of αVβ3 integrin for Vn compared to Fn is compensated on a cellular level when only one ligand is present. Thus, we performed additional experiments to test this hypothesis. First, we tested the dependency of αVβ3 integrin on mechanical force and hybrid domain swing-out for Fn binding on homogenous substrates. Therefore, we cultured β3-wt GFP or β3-N305T GFP expressing NIH3T3 cells on Fn coated cover slips in presence of different concentrations of Y27632 (Fig. S5E). This analysis confirmed that Fn is not an ideal ligand for αVβ3 integrin even when it is the only ligand present (Fig. S5F; also seen in Fig. S2). However, enforced hybrid domain swing-out (β3-N305T) supports stable adhesion formation of αVβ3 integrin on Fn. But even in the context of the β3-N305T mutation cell contractility is needed to support Fn binding as indicated by the Y27632 dependent reduction in adhesion size as shown before (Fig. 3E, G). Next, using live cell imaging, we analyzed cell migration of β1 integrin deficient GD25 cells on substrates homogeneously coated with either Fn or Vn. Cell tracking revealed that cells on Fn

migrated almost two times faster (v_{Fn} = 12.0 ± 3.08 µm/h) compared to cells migrating on Vn (v_{Vn} = 6.7 ± 0.39 µm/h; Video S7). To understand how cell behavior is influenced when GD25 cells can choose between Vn and Fn, we produced stripes of Vn/Fn with cellular resolution (Vn: 20 µm; Fn: 40 µm). Live cell imaging for 12 hrs on these Fn/Vn stripes revealed a turning of cells away from Fn towards Vn (Fig. 5A and Video S8). To quantify this behavior, we measured the surface area of single cells overlying Fn-stripes at different time points (Fig. 5B). 30 min after seeding, cells covered Fn and Vn coated surfaces according to the geometrical coverage (1/3 Vn, 2/3 Fn), indicating a random distribution (Fn/cell colocalization: 67.5%). With increasing time, the surface area of single cells colocalized less with Fn (Fn/cell colocalization after 8 hrs: 28.4%; 24 hrs: 14.6%) demonstrating a preference to adhere to Vn.

Additionally, we asked whether mechanosensing of the extracellular rigidity is affected by the force-dependent ligand binding of αVβ3 integrin. We cultured GD25 cells for 6 hrs on hydrogels with variable stiffness and homogeneously coated with Fn or Vn (Fig. 5C). We measured cell area and the length of paxillin-stained adhesions. Both ligands caused a similar sigmoidal increase of cell area and adhesion length with increasing hydrogel stiffness (Fig. 5D, E). However, cells on Vn showed adhesion maturation and enhanced cell spreading already at 6.7 kPa. Cells on Fn only reached similar plateau values for both parameters at substrates stiffer than 6.7 kPa.

To summarize, we observed that cellular behavior is regulated by the extracellular ligand of αVβ3 integrin. Cell migration and ligand selection experiments indicated that ligand preferences of αVβ3 integrin impact cell behavior and migration. In addition, mechanosensing and mechanotransduction is ligand dependent, implying that force-dependent ligand binding of αVβ3 integrin on Fn substrates requires higher stiffness of the microenvironment than binding of αVβ3 to Vn.

Force-dependent ligand binding is not limited to αVβ3-Fn binding

αVβ3 integrin has been reported to be a highly promiscuous receptor that binds to other ligands besides Fn and Vn, such as fibrinogen (Fbg), osteopontin (Opn), and thrombospondin (Tsp) (Humphries et al., 2006). We therefore produced binary choice substrates to challenge αVβ3 integrin with either Vn/Fbg, Vn/Opn, Vn/Tsp, or Opn/Fn (Fig. S5A-D). On Vn/Fbg and Vn/Tsp αVβ3 integrin preferred to form adhesions on Vn and only revealed 14.7% colocalization to Fbg (Fig 6A) and 6.7% to Tsp (Fig. 6C). In contrast, on Vn/Opn substrates no preference of αVβ3 integrin for one of the ligands could be detected (colocalization to Opn 50.4%; Fig. 6B). Finally, on Fn/Opn substrates, Opn is the preferred binding partner for αVβ3 integrin (colocalization to Opn 81.8%; Fig. 6D) as it was the case with Vn on Fn/Vn substrates. Thus, in the context of binary choice substrates, Opn resembled the preferred αVβ3 integrin ligand Vn, Fbg phenocopied Fn, while Tsp is not a proper ligand for αVβ3 integrin in this context.

Discussion

We have analyzed the interaction of αVβ3 integrin with different ligands by using Fn/Vn binary choice substrates with subcellular geometry, different αVβ3 integrin mutants, and altering cellular contractility. We observed that αVβ3 integrin binds preferentially Vn under a wide range of conditions

while Fn binding required higher cellular contractility. Analyzing different αVβ3 integrin mutations that affect β3 conformation showed that (i) β3-V80C/D241C – interpreted to be locked in extended-closed – binds only Vn and thereby phenocopies αVβ3 integrin in low force conditions, (ii) activating conditions favoring talin association (β3-D723A, β3-VE) do not shift the ratio of Fn/Vn binding, (iii) and that constitutive headpiece opening (β3-N305T + cellular contractility) increases Fn binding. Thus, we introduce a model in which mechanical load on αVβ3 integrin induces a full hybrid domain swing-out to the extended-open conformation via an intermediate extended-primed state (Fig. 6E). During this transition, αVβ3 integrin becomes gradually less selective/more promiscuous by accepting additional ligands like Fn and Fbg. We further show that these ligand-binding properties modulate cellular behavior during spreading, migration, and mechanotransduction depending on the respective ECM protein.

The vitronectin receptor under force

The interaction between αVβ3 integrin, α5β1 integrin, and Fn is intensively studied in different pathological situations and is relevant for morphogenesis (Benito-Jardón et al., 2017; Brunner et al., 2011; van der Flier et al., 2010; Yang et al., 1999). However, αVβ3 was initially described as the 'vitronectin receptor' because of its high Vn-binding properties and, equally important, its inability to bind to Fn (Pytela, Pierschbacher, & Ruoslahti, 1985). How can these contradictory results for αVβ3 integrin be explained? Indeed, under low force conditions (Fig. 2, Fig. S3 F-I), αVβ3 integrin shows high selectivity for Vn and seemingly is the 'vitronectin receptor'. However, the ability of αVβ3 to bind Fn is enhanced by cellular contractility (Fig. 2C, G). This might explain the abundant examples of αVβ3 integrin acting as a Fn-receptor in culture (Elosegui-Artola et al., 2016; Roca-Cusachs et al., 2009; Schiller et al., 2013), or in organisms (Benito-Jardón et al., 2017; Takahashi et al., 2007; van der Flier et al., 2010) in contrast to the force-free assay initially used by Pytela and colleagues (Pytela et al., 1985). All experiments presented here indicate, however, that αVβ3 integrin is rather an auxiliary Fn receptor (at least under cell culture conditions). Yet, this might be a prerequisite for different cellular tasks of αVβ3 and α5β1 integrin in presence of Fn (Roca-Cusachs et al., 2009; Schiller et al., 2013).

Changes in adapter recruitment during adhesion maturation might be an alternative explanation for changes in ligand binding by αVβ3 integrin. Indeed, manipulation of intracellular contractility not only affects force transmission to single integrins but also adhesome composition (Kuo et al., 2011; Schiller, Friedel, Boulegue, & Fässler, 2011). In fact, we showed that vinculin recruitment is needed for increased Fn-binding of αVβ3 integrin. However, to date vinculin is best characterized as a transmitter of force from actin to the talin-integrin axis (Elosegui-Artola et al., 2016; Humphries et al., 2007; Rahikainen et al., 2017). Additionally, recruitment of adhesome proteins to focal adhesions seemed rather unaffected by vinculin knockout (Thievessen et al., 2013). Therefore, we conclude that the effect of vinculin in our experiments is best explained by its role as a force-transmitter. At the same time, we observed that Fn-binding properties of αVβ3 integrin under different force regimes strongly correlate with defined integrin mutations: low mechanical load – extended-closed conformation (β3-V80C/D241C); high mechanical load – extended-open conformation (β3-N305T + force) (Fig 6E). Both of these mutations are extracellular, thereby limiting the potential effects on adapter recruitment. Thus, we propose that force transmission through αVβ3 is necessary for Fn binding.

Structural insights into αVβ3 integrin activation

What is the active (= ligand-binding) conformation of integrins? Recent studies reported for α5β1 integrin an affinity increase from extended-closed to -open conformation by 4 000- to 6 000-fold (Li et al., 2017). This difference makes it likely that the extended-closed conformation of α5β1 integrin is transient and switches directly to extended-open conformation in the presence of ligands. However, this might be different for other integrin receptors. In fact, αIIbβ3 integrin is reported to have an extended-closed/open affinity difference of 'only' 200-fold (Zhu & Springer, 2013). Moreover, the binding of soluble RGD peptides to αIIbβ3 and αVβ3 integrins in extended-closed conformation has been demonstrated in crystal structures (Xiong et al., 2002; Zhu & Springer, 2013). Using a new mutation (β3-V80C/D241C), we provide experimental evidence that αVβ3 integrin in the extended-closed conformation can bind Vn in a cellular environment. Importantly, our observations for αVβ3 integrin are in line with reports about integrin-ligand binding in conformations different from the extended-open state for other integrins (β2 to ICAM (Fan et al., 2019; Fan et al., 2016); αVβ3 to Thy1 (Fiore et al., 2015); αIIbβ3 to Fbg (Chen et al., 2019); α4β7 to MadCAM-1/VCAM-1 (Wang et al., 2018)). Thus, it appears that structure-function relationship of integrins can differ from that of α5β1 integrin. More structural integrin work, potentially with cryo-EM avoiding spatial restrictions of a crystal environment, will help to test this hypothesis.

The need of αVβ3 integrin for complete hybrid domain swing-out in order to bind Fn might also explain the limited effect of classical integrin activators like Mn^{2+}, unclasping the integrin subunits (β3-D723A), or enhancing talin binding (β3-VE; 20-times higher affinity) on changing ligand preference by αVβ3 integrin. It is noteworthy that talin-head binding alone caused integrin extension but not headpiece opening (Ye et al., 2010). The literature for the conformational effects of Mn^{2+} on β3 conformation appears more diverse with findings that Mn^{2+} does not cause headpiece opening at all (Dai et al., 2015), only to 14% (Eng et al., 2011), or for the vast majority of β3 integrins (Miyazaki, Iwasaki, & Takagi, 2018). Our data would support a limited effect of Mn^{2+} on headpiece opening and fits best to studies using integrins including their natural transmembrane domains (Dai et al., 2015; Eng et al., 2011). Additionally, results from FRAP experiments correlate with our observations on Fn/Vn substrates: β3-D723A mutation and Mn^{2+} treatment of β3-wt showed the same FRAP dynamics as β3-wt alone (Cluzel et al., 2005) in contrast to mutations that had an effect on the head-piece opening and on Fn binding (β3-N305T, β3-V80C/D241C, Fig. 4I). Activation by Mn^{2+}, β3-D723A, or β3-VE might instead favor integrin extension and induce a primed state of αVβ3 integrin (Chen et al., 2019; Takagi et al., 2002) but without directly enforcing maximal hybrid domain swing-out.

Regulation of ligand selection

How can αVβ3 integrin select between different ligands that all bind via the RGD sequence (Fn, Vn, Opn, Fbg, Tsp)? The conformation of RGD peptides clearly impacts integrin selectivity given that cyclic RGD is selective for αVβ3 integrin while linear RGD almost equally binds integrin-receptors for Fn and Vn (Pierschbacher & Ruoslahti, 1987). Cormier and colleagues recently argued that ligand binding by αVβ3 integrin might not only be regulated by affinity but also by the accessibility of the ligand to the binding pocket in the integrin headpiece (Cormier et al., 2018). Interestingly, the RGD

motif of Fn is positioned in a rather short loop while Vn and Opn seem to present this motif in a flexible, unstructured protein region. Thus, the limited flexibility of the RGD motif in Fn might cause constraints in accessibility to the binding pocket of αVβ3 integrin dependent on the integrin conformation.

A promiscuous receptor like αVβ3 integrin might encounter potential ligands *in vivo* most of the time. Accordingly, αVβ3 integrin expressing cells might especially benefit from additional ways to regulate ligand binding and selection. So far, we have demonstrated a force-dependent recognition of fibronectin by αVβ3 integrin. Fittingly, αVβ3 integrin – in contrast to α5β1 integrin – is unable to bind soluble fibronectin (Danen, Sonneveld, Brakebusch, Fassler, & Sonnenberg, 2002). At the same time, αVβ3 integrin binds osteopontin from the medium preventing anoikis in melanoma cells (Geissinger, Weisser, Fischer, Schartl, & Wellbrock, 2002). It will be interesting to test additional physiological ligands concerning their dependency on physical parameters like matrix anchorage, solubility, or stiffness for binding to αVβ3 integrin. Influence of these physical parameters on ligand binding will clearly have an impact on pathological settings with altered tissue mechanics like fibrosis, wound healing, or cancer.

Consequences of force-dependent ligand selection

Knockout mice for Fn and for α5 integrin have similar phenotypes (death at E8-8.5 or 9-9.5 (Yang et al., 1999)) indicating that α5β1 integrin is the main Fn receptor during development. In contrast, knockout mice for β3 are viable and fertile (despite showing increased mortality (Hodivala-Dilke et al., 1999)). However, in certain settings αV integrins and αVβ3 in particular are able to compensate for a loss of α5β1-Fn interaction (Benito-Jardón et al., 2017; Takahashi et al., 2007; van der Flier et al., 2010). Endothelial cells depleted in α5 integrin, for example, show increased recruitment of αV integrins to fibronectin fibers (van der Flier et al., 2010). It will be compelling to test whether such an increased recruitment of αVβ3 after α5 reduction is accompanied by increased contractility and/or a changed morphology and altered mechanical characteristics of fibronectin fibers. Interestingly, AFM studies showed that early fibrillogenesis starts already in the cell periphery (Gudzenko & Franz, 2015) where αVβ3 is mostly localized and where high adhesive forces are detected (Kronenberg et al., 2017). Moreover, cancer-associated fibroblasts were reported to reorganize Fn in a multistage process during cancer spheroid invasion with α5β1 and αVβ3 integrin having separate and distinct functions in this process (Attieh et al., 2017; Erdogan et al., 2017). On the other hand, Vn-binding by αVβ3 integrin is an important part of wound healing and inflammation (Keasey et al., 2018) supporting the relevance of ligand selection by αVβ3 integrin. Thus, we expect that force-dependent regulation of ligand promiscuity supports switching between different cellular functions for which we present here a first framework. Combining experiments with controlled presentation of ligands in 2D and 3D (Richter et al., 2017) and experiments mimicking tissues (Franco-Barraza, Beacham, Amatangelo, & Cukierman, 2016; Kaukonen, Jacquemet, Hamidi, & Ivaska, 2017) will be important next steps to understand ligand selection by αVβ3 integrin in more detail.

Acknowledgements:

We thank Marc Hippler for help with atomic force microscopy measurements, Melanie Merkel for help with the analysis of de novo clusters, Deepthy Kavungal for help with cell migration assays, and the bioimaging as well as flow cytometry core facility at the CMU, University of Geneva.

Funding:

This work was supported by the German Research Foundation (Karlsruhe School of Optics and Photonics (KSOP) and BA 6471/1-1 to M. Bachmann) and by the Baden-Württemberg Stiftung (State Scholarship to M. Schäfer). We thank Academy of Finland for financial support (grant no. 290506 to V. Hytönen) and acknowledge CSC – IT center for science for computational resources and EDUFI (former CIMO) for postdoctoral fellowship for V. Mykuliak. Swiss National Science Foundation supported the work of M. Bachmann, M. Ripamonti, and B. Wehrle-Haller (31003A_166384 and 310030L_170112 / 1). The authors declare no competing financial interests.

Figures:

Figure 1: αVβ3 integrin favors binding to vitronectin (Vn) compared to fibronectin (Fn). (**A**) Microcontact printing of 2x2 µm squares of Alexa Fluor 647 labeled Fn (blue) onto glass cover slips and backfilling the pattern with Alexa Fluor 568 labeled Vn (red) leads to differential Fn/Vn patterns (profile along the arrow). Geometrical coverage varies slightly: 44-49% Fn, 56-51% Vn. (**B**) Height profiles of Fn patterns (left) and Fn/Vn patterns (right) measured with atomic force microscopy (AFM) in contact mode. Profiles along the white lines indicate a monolayer of Fn and a uniform topography of the binary choice substrates. (**C**) Super-resolution structured illumination microscopy (SR-SIM) image of NIH3T3 cell transfected with β3-wt GFP integrin (green), cultured on Fn/Vn pattern (Fn blue), and immunostained for paxillin (red). Cell contour is outlined with a dashed white line. (**D**) Quantification of colocalization of β3-wt GFP integrin with Fn or Vn for fixed cells (n = 66; N = 4). (**E**) Representative curves for Fn and Vn association (0 sec to 300 sec) and dissociation (300 sec to 550 sec) to αVβ3 integrin measured *in vitro* with biolayer interferometry. (**F**) Quantification of colocalization of β3-wt GFP integrin with Fn for all adhesions ("general") or only for those bigger than the indicated threshold (re-analysis of the data from **D**). (**G**) Single-cell force spectroscopy of GD25 cells (expressing αVβ3, but no β1 integrin). Detachment forces on Fn and Vn measured after the indicated contact time points. Typically, 10 force measurement repetitions were performed for each cell and time point, and a total of 8 cells were tested. (**H**) NIH3T3 cell transfected with β3-wt GFP integrin (white) seeded on Fn/Vn patterns (Fn blue) was monitored with live cell SR-SIM (Video S1). Magnifications show initiation and maturation of αVβ3-mediated adhesions (time in h:min). Green arrows point to newly established adhesions. Yellow arrows follow adhesions that initiated on Vn while they translocate to Fn. The red arrow at 13 min indicates an adhesion that appeared at the Fn/Vn-interface. (**I**) Total number of αVβ3-mediated adhesions that initiated on Vn, Fn, or at the Fn/Vn-interface for cells imaged with live cell SR-SIM. Quantification is based on 246 initiated adhesions from six cells out of three independent experiments. (**C, H**) Scale bars: 10 µm in overviews, 2 µm in zoom-ins; 5 µm in (**A**).

Figure 2: Cell contractility regulates ligand preference of αVβ3 integrin. (**A**) NIH3T3 cells transfected with β3-wt GFP integrin (green) were cultured on Fn/Vn substrates (Fn in blue) in the presence of 10 µM blebbistatin and were stained after fixation for actin (red). (**B**) NIH3T3 cells treated with 10 µM Y27632. (**C**) NIH3T3 cells transfected with β3-wt GFP integrin (green) and myosin IIA mApple (NMIIA; red) with serum (FCS; 10 %) present in the medium. (**D**) MEF wt or (**E**) MEF vinculin knockout cells (MEF Vcl -/-) transfected with β3-wt GFP integrin (green) and immunostained for paxillin (Pxn; red). (**F**) MEF Vcl -/- cells transfected with β3-wt GFP integrin (green) and Vcl mCherry (red). (**G**) Quantifications of colocalization of β3-wt GFP with Fn for cells treated as described in **A-C** (control + FCS: n = 66, N = 3; control + DMSO: n = 46, N = 3; + 10 µM blebbistatin: n = 40, N = 3; + 10 µM Y-27632: n = 54, N = 3; + NMIIA mCherry: n = 55, N = 3). (**H**) Quantifications of colocalization of β3-wt GFP with Fn for cells treated as described in **D-F** (control: n = 38, N = 3; MEF Vcl -/-: n = 57, N = 3; MEF Vcl -/- + Vcl mCherry: n = 42, N = 3). (**A-F**) All fluorescent images were acquired with SR-SIM. White dashed lines indicate cell outline. Scale bar: 10 µm in overview images, 2 µm in zoom ins.

Figure 3: Hybrid domain swing-out is necessary for αVβ3 integrin binding to FN. (**A**) NIH3T3 cell transfected with β3-wt GFP integrin (green). 1 mM Mn^{2+} was added to the medium 30 min before fixation. (**B**) NIH3T3 cell transfected with β3-VE GFP integrin (green), or (**C**) with β3-D723A GFP integrin (green), or (**D**) with β3-N305T GFP integrin (green). (**E**) β3-N305T GFP integrin transfected cells treated with 10 µM blebbistatin. All cells (**A-E**) were fixed and immunostained for paxillin (Pxn; red). Zoom-ins depict adhesions in the cellular periphery (1) or the cell center (2). (**F**) Quantifications of colocalization of β3 GFP with Fn for cells treated as described in **A-D** and imaged with SR-SIM. Paxillin was used as a mask to exclude αVβ3 integrin clusters in the cell center from analysis (β3-wt: replot of the data from Fig. 1D; β3-wt + Mn2+: n = 55, N = 3; β3-VE: n = 54, N = 3; β3-D723A: n = 43, N = 3; β3-N305T: n = 66, N = 4). (**G**) Quantification as described in **F** for cells treated as described before. Data for 'β3-N305T + Mn2+' was acquired from cells treated as described in **D** but with addition of 1 mM Mn^{2+} for the last 30 min before fixation. All images were acquired with diffraction-limited microscopy (β3-wt: n = 40, N = 3; β3-N305T: n = 42, N = 3; β3-N305T + Blebb: n = 39, N = 3). (**H**) Superimposition of (gray) the initial structure of αVβ3 integrin, (blue) the same structure after 100 ns molecular dynamics (MD) simulation, and (red) the N303-glycosylated structure after 100 ns MD simulation. Cyan lines indicate the position of hybrid domain swing-out measurements. (**I**) Fluctuation of the angle γ between βI-like and hybrid domain over time during the MD simulation. (**J**) Live cell SR-SIM imaging of a NIH3T3 cell transfected with β3-N305T GFP integrin (white) spreading on Fn/Vn substrates (Fn in blue). Yellow arrows indicate an αVβ3 integrin-mediated adhesion that initiated on Fn. (**K**) Number of αVβ3 integrin-mediated adhesions per cell that initiated on Fn for NIH3T3 cells transfected with the indicated integrin (β3-wt is a replot of the data in Fig. 1I; β3-VE: six cells analyzed out of three independent experiments; β3-N305T: six cells analyzed out of four independent experiments). (**L**) Superimposition of αVβ3 integrin structures as described in (**H**) for β3-wt (blue) and β3-glycosylated (red). Fully activated structures were created based on PBD: 4MMX with an arranged hybrid domain swing-out according to (Fully activated 1, green) PBD: 3EZ2, or (Fully activated 2, orange) PBD: 3FCU. (**A-E, J**) Scale bars: overview images 10 µm, zoom-ins 2 µm. White dashed lines indicate cell outline. Images were acquired with (**A-D, J**) SR-SIM or (**E**) diffraction limited microscopy.

Figure 4: Extended-closed mutant β3-V80C/D241C binds Vn but not Fn. (**A**) Structural analysis of the distance between V80 and D241 for extended-closed conformation of αVβ3 integrin (left; PBD: 4MMX) after introducing a V80C/D241C disulfide bridge, (middle) for the wt structure, or (right; PBD: 4MMX; hybrid domain swing-out arranged based on 3FCU) for the extended-open conformation. (**B-E**) NIH3T3 cells transfected with β3-V80C/D241C GFP (green) cultured on the indicated ECM proteins for 2 hrs. 1 mM Mn^{2+} was added for the last 30 min where indicated. Cells were stained for paxillin (red) and actin (blue) after fixation. Please note the absence of αVβ3 integrin clustering on Fn and the increased localization of β3-V80C/D241C in adhesions on Vn for Mn^{2+} treated compared to untreated cells. (**F, G**) Cells were prepared as described in **B-E** except that they were cultured on Fn/Vn substrates. (**H**) Quantifications of colocalization of β3 GFP with Fn for cells treated as described **G** (β3-wt: replot of the data from Fig. 3G; β3-V80C/D241C + Mn2+: n = 29, N = 3). (**I**) NIH3T3 cells were transfected with the indicated plasmids and cultured on serum coated cover slips for 15-20 hrs. FRAP measurement of αVβ3 integrin dynamics for the indicated conditions (β3-wt: n = 40, N = 3; β3-N305T: n = 48, N = 3; β3-V80C/D241C: n = 36, N = 3). (**B-G**) Scale bars: overview images 10 µm, zoom-ins 2

µm. White dashed lines indicate cell outline. Fluorescent images were taken (**B-G**) with diffraction limited microscopy.

Figure 5: The preference of αVβ3 integrin for Vn influences cellular behavior. (**A**) GD25 cells (no β1 expression) were seeded onto stripe assays of stamped Vn (red; 20 µm) backfilled with Fn (40 µm). Alexa Fluor 647 labeled Vn was added to visualize Vn stripes. GD25 cells were visualized with phase contrast microscopy for 12 hrs. (**B**) Quantification of the colocalization of GD25 cells with Fn on Vn/Fn stripe assays at the indicated time points. The first time point was quantified based on phase contrast movies as shown in (**A**) while 8 hrs and 24 hrs time points were calculated from experiments with cells cultured in the incubator, fixed, and stained for actin (0.5h: n = 123, N = 3; 8h: n = 17, N = 3; 24h: n = 15, N = 3 (**C-E**) GD25 were cultured for 6 hrs on polyacrylamide gels of the indicated Young's modulus (E) and stained for paxillin (red) and actin (green). Gels were coated homogeneously with Vn or with Fn. (**C**) Cells on 6.7 kPa hydrogels showed less cell spreading and adhesion maturation on Fn coated substrates compared to Vn. (**D**) Length of paxillin-stained adhesions (longest 10% only to indicate matured adhesions) or (**E**) cell area was plotted against the Young's modulus for cells on Vn (black data points) or Fn (blue data points; see Table S1 for number of analyzed cells; p-values except the indicated: $p > 0.1$; see also Table S2). All cells were imaged with diffraction limited microscopy. (**A, C**) Scale bar: 10 µm in overviews, 2 µm in zoom-ins.

Figure 6: Osteopontin (Opn) phenocopies Vn, fibrinogen (Fbg) phenocopies Fn in binary choice substrates. (**A-D**) β3-wt GFP was expressed in NIH3T3 cells that were cultured on alternative binary choice substrates (Fig. S5 A-D). Quantification of the colocalization of β3-wt GFP with indicated ECM proteins for cells cultured on Vn/Fbg (n = 57, N = 3), Vn/Opn (n = 45, N = 3), Vn/Tsp (n = 34, N = 3), or Fn/Opn (n= 53, N = 3). (**E**) Model for force-dependent differential ligand binding of αVβ3: αVβ3 integrin is in equilibrium between bent and extended conformations. Integrin mutations may stabilize the integrin in intermediate conformations identified in a multistep activation process (for example β3-N305T without force: step 7 of 8 (Zhu & Springer, 2013); N303-glycosylation: gray square between βI and hybrid domain). Headpiece opening (indicated with red angle) is decisive for Fn binding while Vn stays the preferred αVβ3 integrin ligand. Binding of Vn presumably precedes force mediated headpiece opening that requires a ligand-integrin-actin axis to act on αVβ3 integrin. FRAP measurements indicate that low FRAP dynamics facilitate Fn binding (low off-rate of β3-N305T indicated by smaller equilibrium-arrow from extended-open back to -primed). Thus, mechanical forces favor the full αVβ3 integrin activation that enables stable binding to additional ligands and enhances thereby ligand promiscuity of αVβ3 integrin.

Methods:

Cell culture, constructs, and transfection

NIH3T3 cells used in this study are a subclone of NIH3T3 cells (ATCC, CRL-16589) that were FACS sorted for low expression of endogenous β3-integrin as described pr)viously (Pinon et al., 2014). Vinculin-knockout mouse embryonic fibroblasts (MEF Vcl -/-) and MEF wt were kindly provided by W. H. Ziegler (Mierke et al., 2010). GD25wt cells were kindly provided by R. Fässler (Wennerberg et al., 1996). All cells were grown at 37°C with 5% CO_2 in DMEM (ThermoFischer) supplemented with 10% FCS (Hyclone), and passaged 2-3 times a week, or upon reaching confluency. Transfections were carried out with Lipofectamine 2000 (ThermoFischer) or JetPEI (Polyplus) according to manufacturer's instructions. Cells were cultured in complete medium for 48 hrs before detachment. cDNA encoding full-length mouse β3-wt GFP integrin expressed in a cytomegalovirus promoter-driven pcDNA3/EGFP vector has been previously described (Ballestrem, Hinz, Imhof, & Wehrle-Haller, 2001). β3-VE GFP (Pinon et al., 2014), β3-D723A GFP (Ballestrem et al., 2001), and β3-N305T GFP (Ballestrem et al., 2001) were derived by substitution from the β3-wt GFP integrin construct mentioned before and as described in the indicated publications. Vinculin mCherry was a gift from Christoph Ballestrem (Manchester, UK), and mApple-MyosinIIA-C-18 was a gift from Michael Davidson (Addgene plasmid # 54929).

Antibodies and chemicals

Inhibition experiments were performed with blebbistatin (Sigma-Aldrich), with the ROCK inhibitor Y27632 (Sigma-Aldrich), or with the αVβ3 integrin inhibitor cilengitide (Sellekchem) at concentrations as indicated. Dithiothreiol (DTT, Carl Roth) was used at the indicated concentration to open disulphide bridges. Cells were fixed for subsequent immunostaining with 4% PFA (Sigma-Aldrich) in PBS. Reagents used for immunostaining were monoclonal mouse antibodies for paxillin (1:1000, clone 349/Paxillin, BD Biosciences, # 610052), talin (clone 8d4, Sigma-Aldrich, #T3287), vinculin (clone hVIN-1, abcam, #ab11194), vitronectin (1:1000, clone VIT-2, IgM, Sigma-Aldrich, #V7881) or polyclonal rabbit antibodies for HA-tag (Sigma-Aldrich, #H6903), fibronectin (1:500, Sigma-Aldrich, #F3648), thrombospondin (abcam, #ab85762) or osteopontin (GeneTex, #GTX37582). β1-integrin was stained with a monoclonal rat antibody (1:100, clone 9EG7, BD Biosciences, # 553715). After primary antibody staining, samples were washed and incubated with antibodies against mouse labeled with Cy3 (1:500, Jackson Immunoresearch, #115-165-146), against rabbit labeled with Alexa Fluor 488 (1:500, ThermoFischer, #A11070) or Cy3 (1:500, Dianova, #111-165-144), or with phalloidin coupled to Alexa Fluor 568 (1:200, ThermoFischer, #A12380). To visualize anti-Vn staining, secondary antibodies against IgM labeled with Cy3 were used (1:1000, Dianova, #115-166-075). Primary rat antibodies were visualized with preadsorbed, Alexa Fluor 488 or Alexa Fluor 568 labeled secondary antibodies (1:500, ThermoFischer, #A11006 or #A11077) and, if present in the experiment, primary mouse antibodies were visualized with preadsorbed, Cy3 labeled antibodies (1:500, Dianova, #111-165-144) to avoid cross-reactivity of secondary antibodies. Direct labeling of Fn, Fbg, and Vn was performed according to manufacturer's protocol with Alexa Fluor 568 (ThermoFischer, # A10238) or Alexa Fluor 647 (ThermoFischer, #A20173).

Microcontact printing

Silicone stamps for microcontact printing of differential substrates were produced as previously described (Lehnert et al., 2004). Binary choice susbtrates were produced with human plasma fibronectin (Sigma-Aldrich, #F2006 or Millipore, #FC010), human plasma vitronectin (Sigma-Aldrich, #V8379), recombinant human vitronectin (Sigma-Aldrich, #SRP3186), native human fibrinogen (Bio-Rad, #4440-8604), recombinant human thrombospondin-1 (R&D systems, #3074-TH-050), or with osteopontin from bovine milk (Sigma-Aldrich, #O3514).

Fn/Vn substrates: Silicone stamps were incubated for 10 min with a solution containing: (i) Alexa Fluor 647 labeled Fn (depending on labeling degree; typically, 2.5-3 µg/ml Fn-647 were used), (ii) 5 µg/ml Fn, and (iii) 45 µg/ml heat-inactivated Fn in PBS (Fn-X, see Fig. S1E). Heat-inactivated Fn was produced by heating Fn for 30 min to 90°C. Cells do not spread on heat-inactivated Fn (Fig. S1E). After nitrogen drying of the stamp with the adsorbed Fn, the stamp was pressed onto a glass cover slip for 10 min before the stamp was released. Next, the pattern on the cover slip was covered with Vn at a concentration of 1-5 µg/ml in PBS for 1 hour at room temperature. High concentrations of the stamped protein (Fn in this case, with 50 µg/ml total Fn + 2.5-3 µg/ml Fn-647) improved the reproducibility of the patterns by preventing adsorption of the backfilled protein (Vn in this case) to the stamped areas.

For other binary choice substrates than Fn/Vn, a total concentration of 50 µg/ml of the stamped protein, and 5 µg/ml of the backfilled protein was used. The only exception is the Vn/Fn stripe pattern shown in Fig. 5A where 10 µg/ml for both proteins were used. All other steps for stripe patterns were performed as described. After the final incubation step, patterns were washed with PBS and used directly for cell seeding. Cell detachment from culture flasks was stopped with trypsin inhibitor (Sigma-Aldrich) and cells were cultured in absence of FCS if not stated otherwise. However, Fig. 2G indicated that FCS adsorption was negligible on Fn/Vn patterns during a 2 hrs incubation period.

Polyacrylamide gels

Established protocols (Kandow, Georges, Janmey, & Beningo, 2007; Pinon et al., 2014; Plotnikov, Sabass, Schwarz, & Waterman, 2014) were adapted to gain polyacrylamide gels of different Young's modulus (stiffness) with homogeneous or with structured ECM. Gels were produced on activated cover slips: glass cover slips were cleaned with propanol and for 10 min in a plasma cleaner (Technics Plasma GmbH, Germany). This was followed by a silanization (1 h at room temperature, 1 mM 3-(Trimethoxysilyl)propyl methacrylate (Sigma-Aldrich) in toluene). After incubation, cover slips were washed in ddH_2O and dried with nitrogen. On these cover slips, 60 µl of a mixture of degassed acrylamide, bisacrylamide (both Bio-Rad), tetramethylethylenediamine, and ammonium persulfate (TEMED and APS; Sigma-Aldrich) was pipetted with final concentrations of 0.5% APS, 0.1% TEMED, and as mentioned in Table S1. This solution was covered with 10 µl of 1% w/v of Acrylic acid *N*-hydroxysuccinimide ester (NHS acrylate; Sigma-Aldrich) in toluene. Finally, the solution was covered with a cover slip of 18 mm diameter that was either functionalized with a Fn/Vn pattern prepared as described before or that was coated with a 50 µg/ml solution of Fn or Vn for 1h at room temperature. This top cover slip was dried with nitrogen before it was applied to the gel solution. After

polymerization of the polyacrylamide gel, the top cover slip was removed and the gel was covered with PBS. Gel substrates were used directly for cell seeding or were stored overnight at 4°C before cell seeding. Cells were cultured for 6 hrs on gels in DMEM without FCS to prevent adsorption of plasma-Vn to the gel surface.

Stiffness of polyacrylamide gels was measured as previously described (Elosegui-Artola et al., 2016). Measurements were performed with the atomic force microscope described below. Silicon nitride pyramidal tips with a nominal spring constant of k = 0.01-0.03 Nm^{-1} were used (MLCT, Bruker). An effective half-angle of 20° was used for calculation. For each stiffness, 3 gels from 3 independent batches were measured by probing 5 positions in the center of the gel with 5 repetitive measurements. The Hertz model equation for pyramidal tips was fitted to the force-displacement curves.

Microscopy

SR-SIM imaging was performed on a non-serial Zeiss Elyra PS.1 microscope with a 63x/1.4NA oil immersion objective and an Andor iXon EMCCD camera. The grid for SR-SIM was rotated three times and shifted five times leading to 15 frames raw data out of which a final SR-SIM image was calculated with the structured illumination package of ZEN software (Zeiss). Values for calculation were selected for best resolution without causing image artifacts. Channels were aligned by using a correction file that was generated by measuring channel misalignment of fluorescent tetraspecs (ThermoFischer, #T7280). All diffraction limited images according to the figure legend were taken using the ApoTome module on a Zeiss AxioimagerZ1 microscope to achieve optical sectioning. A 63x/1.4NA oil immersion objective and a Zeiss AxioCam MRm were used. For SR-SIM live cell microscopy, the incubation chamber was heated to 37°C and cells were imaged every minute. During imaging, cells were cultured in imaging medium (F12 + 25 mM HEPES + 200 mM L-glutamine + 1% penicillin/streptomycin, pH 7.2). FCS was present as indicated in the description of the Supplementary Movies. SIM raw data images were processed as described above. Phase contrast live cell imaging was performed on a Zeiss Axio-Observer Z.1 with a 20x/0.8NA air objective. Cell migration of GD25 cells on homogenous Fn or Vn (coating: 10 µg/ml in PBS for 1h at RT) was analyzed for cells cultured in DMEM/F12 medium (ThermoFischer, #11039-021) + 1% penicillin/streptomycin + 1% FCS. Migration of GD25 cells on Vn/Fn stripes was analyzed for cells cultured in DMEM/F12 medium + 1% penicillin/streptomycin.

FRAP

Fluorescence Recovery After Photobleaching (FRAP) was performed as described (Wehrle-Haller, 2007). Image acquisition and image analysis were performed at the Bioimaging Core Facility, Faculty of Medicine, University of Geneva. Briefly, transfected NIH3T3 cells were cultured on serum coated coverslips. 1 h before imaging medium was replaced with F12 medium (Sigma-Aldrich) containing 10% FCS + 1% penicillin/streptomycin and cells were relocated to the microscope. FRAP was performed on a Nikon A1r confocal laser scanning microscope equipped with a 60x oil immersion objective and a 37°C incubation chamber. Three pictures in 5 sec intervals were acquired before bleaching. After that we acquired 1 frame / 5 sec for 3 min. The graph was calculated in the following way: The first three images before bleaching were averaged to yield “100% intensity” and the first

image after bleaching was set to “0% intensity”. All other values were calculated as ratio of 100% intensity.

Atomic Force Microscopy

To prepare adhesion substrates for directly comparative adhesion force spectroscopy, adjacent areas on a Fluorodish 35 (WPI) glass bottom dish were coated with 50 µg/ml BSA (to provide low adhesion for cell capture, see below), 50 µg/ml Fn, or 5 µg/ml Vn solutions and incubated for 1h. Substrates were subsequently rinsed five times with PBS and transferred to CO_2-independent Medium (ThermoFischer). Prior to SCFS experiments, GD25 cells were transferred to CO_2-independent Medium for 1 h and then trypsinized. Trypsin was subsequently inactivated by adding soybean trypsin inhibitor (Sigma-Aldrich). After centrifugation, the supernatant was removed, and cells were again resuspended in CO_2-independent Medium. SCFS experiments were performed using a CellHesion 200 atomic force microscope (JPK) featuring an extended vertical range of 100 µm. All measurements were performed at 37ºC using a temperature-controlled sample chamber (BioCell from JPK) and tipless 205 µm long V-shaped cantilevers with a nominal spring constant of 0.06 N/m (NP-O from Veeco). To facilitate cell capture, plasma-cleaned cantilevers were functionalized with concanavalin A. After calibrating the sensitivity of the optical lever system and determining the spring constant, cells were pipetted into the sample chamber. A single cell was captured above the BSA coated area by pressing the functionalized cantilever onto the cell with a contact force of 500 pN for 3 s and elevating the cantilever subsequently. To measure cell detachment forces, the cantilever was lowered at a constant speed of 5 µm/s until the cell made contact with the substrate and a preset force of 1.5 nN was reached. Afterwards, the cantilever was held at a constant height for the preset contact time until the cantilever was elevated 80 µm above the substrate surface. Each cell was tested alternatingly on Fn and Vn surfaces (typically 10 force cycle repetitions for each contact time) to determine the differential adhesion strength to both ligands. In total, 8 different cells were tested. Detachment forces were analyzed using the JPK image processing software. From the collected force-distance curves, the maximum detachment forces (maximum cantilever deflection) were determined and plotted as mean ± SD using OriginPro 8.1G. Statistical significance of experiments was tested with a Wilcoxon-based Mann-Whitney U-test using InStat.

Image Analysis

Colocalization, cell area, and adhesion length were analyzed with the Fiji software package (Schindelin, Rueden, Hiner, & Eliceiri, 2015). A threshold was applied to the intensity of the corresponding fluorescent channel and the area or the length of individual integrin-mediated adhesions was measured with plugins included in Fiji. If necessary, background was subtracted (sliding paraboloid) or analysis was limited to adhesions in areas with less background. Colocalization between two fluorescent channels was quantified by measuring Mander’s coefficient of thresholded images by using the Fiji plugin JACoP (Bolte & Cordelieres, 2006). The location of adhesion initiation on Fn/Vn substrates was defined by analyzing SR-SIM live cell movies. The fluorescent channel of the integrin staining was analyzed while the Fn channel was hidden. Integrin clusters visible for at least two subsequent time frames were marked with an ellipse in the ZEN imaging software throughout the movie. Afterwards, the Fn channel was uncovered, and the positions of all ellipses were counted with

respect to FN squares or Vn surrounding the squares. If an integrin cluster initiated at the border of a square with contact to Fn and Vn, it was counted for the category ‘Fn/Vn’.

Biolayer interferometry measurement

Binding and unbinding behavior of αVβ3 integrin binding to different ECM proteins were measured using the BLItz biolayer interferometer (Pall ForteBio). All steps during real-time measurements were performed at room temperature in the same buffer conditions (20 mM Tris, 150 mM NaCl, pH 7.4, 1mM $MgCl_2$, 1 mM $CaCl_2$, 0.02% Tween20, 0.1% BSA). Pre-hydrated (10 minutes in integrin buffer) Ni-NTA biosensors (Pall ForteBio) were loaded with 50 µg/ml His-tagged human recombinant αVβ3 integrin (RnD Systems, #3050-AV) following an association phase with 150 µg/ml ECM protein and a dissociation phase (time scheme: baseline – 45 s; loading – 180 s; baseline – 45 s; association – 300 s, dissociation – 250 s). Binding curves were corrected for a reference sample: an integrin loaded biosensor was used without adding ligand in the association phase (to correct for drift of the system and unspecific bound buffer components). In control experiments (Fig. S3E), 20 µM cilengitide was added to the integrin buffer during dissociation phase. A 10 s adjustment step was included.

MD simulations

Crystal structure of αVβ3 integrin from RCSB Protein Data Bank (PDB: 4MMX) was used as a model for the extended-closed integrin. Structure of the extended-open form was prepared by superimposition of βI-like and hybrid domains from the crystal structure of open αIIbβ3 integrin (PDB: 3FCU or PDB: 3ZE2 as indicated in the figure legend). Systems containing unliganded αVβ3 were prepared by removing FnIII10 from initial structure. Glycoyslation of β3 integrin at N303 was achieved by covalently attaching four sugar rings to nitrogen atom of the N303 residue. Preparation of structures and analysis was performed using PyMOL 1.7. MD simulations were performed using Gromacs ver 2016.5 (Van Der Spoel et al., 2005) at the Sisu supercomputer, CSC, Finland. The Amber ff99SB-ILDN force field (Lindorff-Larsen et al., 2010) and explicit TIP3P water model (Jorgensen & Madura, 1983) were used. The total system charge was neutralized with K+ ions. The parameters for the glycosylation part were prepared using ACPYPE (Sousa da Silva & Vranken, 2012). Energy minimization of the system was performed in 25 000 steps using steepest descent algorithm. The system was equilibrated in three phases using harmonic position restraints on all heavy atoms of protein. The first phase of equilibration was performed with NVT ensemble for 100 ps using the Berendsen weak coupling algorithm (Berendsen, Postma, Gunsteren, DiNola, & Haak, 1984) to control the temperature of the system at 100 K. Integration time step of 2 fs was used in all the simulations. Following NVT, the system is linearly heated from 100 to 310 K over 1 ns using an NPT ensemble at 1 atm of pressure. During this process, the Berendsen algorithm was used to control both temperature and pressure. For the final phase of equilibration and for all subsequent simulations, an NPT ensemble was maintained at 310 K, using V-rescale algorithm (Bussi, Donadio, & Parrinello, 2007), and 1 atm using Berendsen algorithm. Temperature coupling was applied separately for protein and solution parts.

Flow-cytometric β3 integrin activation index

NIH3T3 cells were transfected with JetPrime (Polyplus) and the indicated β3 plasmids according to the manufacturer's protocol. Cells were detached after 48 hrs and split into two groups. One was stained with hamster anti-mouse β3 integrin (1:500, clone HMβ3-1, BD #550541) and goat anti-hamster phycoerythrin (1:600, Jackson Immunoresearch, #127-115-160). The other group of cells was incubated with a fusion protein of CD31 and the RGD-containing ligand soluble Kistrin-7 (Ski7; used 1:5 as supernatant from cell culture) followed by staining for CD31 with rat anti-CD31 (1:50, clone GC51, supernatant) and goat anti-rat phycoerythrin staining (1:800, Jackson Immunoresearch, #112-116-143). All reagents were diluted in PBS + 1% BSA and incubations were performed for 30 min on ice. Cells were washed by centrifugation and resuspending of the pellet in fresh, ice-cold PBS 2x before every incubation and after the last incubation. Before cytometric analysis, cell pellets were resuspended in PBS + 1% BSA + 1 mM EDTA. All analyses were performed on an Accuri C6 and data was analyzed with FlowJo (BD). After bleed-through correction and gating for viable, transfected single cells, median values of PE staining were calculated for total β3 and Ski7-stained β3. The ratio Ski7/total staining was calculated and normalized to the activation ratio of β3-wt GFP.

Statistics

If not stated otherwise, reported values in bar charts are calculated as mean and error bars are representing standard deviation of all data points. In box plots, upper and lower bar indicate standard deviation and the middle bar indicates the mean. Statistical comparisons are calculated with two-tailed Student's t-test based on the number of independent experiments. For adhesion force measured with AFM, statistical significance of experiments was tested with a Wilcoxon-based Mann-Whitney U-test using InStat. All experiments were reproducible and were carried out as independent experiments at least twice or as often as indicated in the figure legends.

References:

Attieh, Y., Clark, A. G., Grass, C., Richon, S., Pocard, M., Mariani, P., . . . Vignjevic, D. M. (2017). Cancer-associated fibroblasts lead tumor invasion through integrin-beta3-dependent fibronectin assembly. *J Cell Biol*. doi:10.1083/jcb.201702033

Bachmann, M., Kukkurainen, S., Hytönen, V. P., & Wehrle-Haller, B. (2019). Cell Adhesion by Integrins. *Physiol Rev, 99*(4), 1655-1699. doi:10.1152/physrev.00036.2018

Ballestrem, C., Hinz, B., Imhof, B. A., & Wehrle-Haller, B. (2001). Marching at the front and dragging behind: differential alphaVbeta3-integrin turnover regulates focal adhesion behavior. *J Cell Biol, 155*(7), 1319-1332. doi:10.1083/jcb.200107107

Benito-Jardón, M., Klapproth, S., Gimeno-LLuch, I., Petzold, T., Bharadwaj, M., Müller, D. J., . . . Costell, M. (2017). The fibronectin synergy site re-enforces cell adhesion and mediates a crosstalk between integrin classes. *Elife, 6*. doi:10.7554/eLife.22264

Berendsen, H. J. C., Postma, J. P. M., Gunsteren, W. F. v., DiNola, A., & Haak, J. R. (1984). Molecular dynamics with coupling to an external bath. *The Journal of Chemical Physics, 81*(8), 3684-3690. doi:10.1063/1.448118

Bolte, S., & Cordelieres, F. P. (2006). A guided tour into subcellular colocalization analysis in light microscopy. *J Microsc, 224*(Pt 3), 213-232. doi:10.1111/j.1365-2818.2006.01706.x

Brunner, M., Millon-Frémillon, A., Chevalier, G., Nakchbandi, I. A., Mosher, D., Block, M. R., . . . Bouvard, D. (2011). Osteoblast mineralization requires beta1 integrin/ICAP-1-dependent fibronectin deposition. *J Cell Biol, 194*(2), 307-322. doi:10.1083/jcb.201007108

Bussi, G., Donadio, D., & Parrinello, M. (2007). Canonical sampling through velocity rescaling. *J Chem Phys, 126*(1), 014101. doi:10.1063/1.2408420

Byron, A., Humphries, J. D., Bass, M. D., Knight, D., & Humphries, M. J. (2011). Proteomic analysis of integrin adhesion complexes. *Sci Signal, 4*(167), pt2. doi:10.1126/scisignal.2001827

Campbell, I. D., & Humphries, M. J. (2011). Integrin structure, activation, and interactions. *Cold Spring Harb Perspect Biol, 3*(3). doi:10.1101/cshperspect.a004994

Chen, Y., Ju, L. A., Zhou, F., Liao, J., Xue, L., Su, Q. P., . . . Zhu, C. (2019). An integrin α. *Nat Mater, 18*(7), 760-769. doi:10.1038/s41563-019-0323-6

Chillakuri, C. R., Jones, C., & Mardon, H. J. (2010). Heparin binding domain in vitronectin is required for oligomerization and thus enhances integrin mediated cell adhesion and spreading. *FEBS Lett, 584*(15), 3287-3291. doi:10.1016/j.febslet.2010.06.023

Cluzel, C., Saltel, F., Lussi, J., Paulhe, F., Imhof, B. A., & Wehrle-Haller, B. (2005). The mechanisms and dynamics of (alpha)v(beta)3 integrin clustering in living cells. *J Cell Biol, 171*(2), 383-392. doi:10.1083/jcb.200503017

Cormier, A., Campbell, M. G., Ito, S., Wu, S., Lou, J., Marks, J., . . . Cheng, Y. (2018). Cryo-EM structure of the alphavbeta8 integrin reveals a mechanism for stabilizing integrin extension. *Nat Struct Mol Biol, 25*(8), 698-704. doi:10.1038/s41594-018-0093-x

Dai, A., Ye, F., Taylor, D. W., Hu, G., Ginsberg, M. H., & Taylor, K. A. (2015). The Structure of a Full-length Membrane-embedded Integrin Bound to a Physiological Ligand. *J Biol Chem, 290*(45), 27168-27175. doi:10.1074/jbc.M115.682377

Danen, E. H., Sonneveld, P., Brakebusch, C., Fassler, R., & Sonnenberg, A. (2002). The fibronectin-binding integrins alpha5beta1 and alphavbeta3 differentially modulate RhoA-GTP loading, organization of cell matrix adhesions, and fibronectin fibrillogenesis. *J Cell Biol, 159*(6), 1071-1086. doi:10.1083/jcb.200205014

Dao, L., Weiland, U., Hauser, M., Nazarenko, I., Kalt, H., Bastmeyer, M., & Franz, C. M. (2012). Revealing non-genetic adhesive variations in clonal populations by comparative single-cell force spectroscopy. *Exp Cell Res, 318*(17), 2155-2167. doi:10.1016/j.yexcr.2012.06.017

Elosegui-Artola, A., Oria, R., Chen, Y., Kosmalska, A., Perez-Gonzalez, C., Castro, N., . . . Roca-Cusachs, P. (2016). Mechanical regulation of a molecular clutch defines force transmission and transduction in response to matrix rigidity. *Nat Cell Biol, 18*(5), 540-548. doi:10.1038/ncb3336

Eng, E. T., Smagghe, B. J., Walz, T., & Springer, T. A. (2011). Intact alphaIIbbeta3 integrin is extended after activation as measured by solution X-ray scattering and electron microscopy. *J Biol Chem, 286*(40), 35218-35226. doi:10.1074/jbc.M111.275107

Engler, A. J., Chan, M., Boettiger, D., & Schwarzbauer, J. E. (2009). A novel mode of cell detachment from fibrillar fibronectin matrix under shear. *J Cell Sci, 122*(Pt 10), 1647-1653. doi:10.1242/jcs.040824

Erdogan, B., Ao, M., White, L. M., Means, A. L., Brewer, B. M., Yang, L., . . . Webb, D. J. (2017). Cancer-associated fibroblasts promote directional cancer cell migration by aligning fibronectin. *J Cell Biol*. doi:10.1083/jcb.201704053

Fan, Z., Kiosses, W. B., Sun, H., Orecchioni, M., Ghosheh, Y., Zajonc, D. M., . . . Ley, K. (2019). High-Affinity Bent β. *Cell Rep, 26*(1), 119-130.e115. doi:10.1016/j.celrep.2018.12.038

Fan, Z., McArdle, S., Marki, A., Mikulski, Z., Gutierrez, E., Engelhardt, B., . . . Ley, K. (2016). Neutrophil recruitment limited by high-affinity bent β2 integrin binding ligand in cis. *Nat Commun, 7*, 12658. doi:10.1038/ncomms12658

Fernandez-Sauze, S., Grall, D., Cseh, B., & Van Obberghen-Schilling, E. (2009). Regulation of fibronectin matrix assembly and capillary morphogenesis in endothelial cells by Rho family GTPases. *Exp Cell Res, 315*(12), 2092-2104. doi:10.1016/j.yexcr.2009.03.017

Fiore, V. F., Strane, P. W., Bryksin, A. V., White, E. S., Hagood, J. S., & Barker, T. H. (2015). Conformational coupling of integrin and Thy-1 regulates Fyn priming and fibroblast mechanotransduction. *J Cell Biol, 211*(1), 173-190. doi:10.1083/jcb.201505007

Franco-Barraza, J., Beacham, D. A., Amatangelo, M. D., & Cukierman, E. (2016). Preparation of Extracellular Matrices Produced by Cultured and Primary Fibroblasts. *Curr Protoc Cell Biol, 71*, 10.19.11-10.19.34. doi:10.1002/cpcb.2

Geissinger, E., Weisser, C., Fischer, P., Schartl, M., & Wellbrock, C. (2002). Autocrine stimulation by osteopontin contributes to antiapoptotic signalling of melanocytes in dermal collagen. *Cancer Res, 62*(16), 4820-4828.

George, E. L., Georges-Labouesse, E. N., Patel-King, R. S., Rayburn, H., & Hynes, R. O. (1993). Defects in mesoderm, neural tube and vascular development in mouse embryos lacking fibronectin. *Development, 119*(4), 1079-1091.

Gladson, C. L., Wilcox, J. N., Sanders, L., Gillespie, G. Y., & Cheresh, D. A. (1995). Cerebral microenvironment influences expression of the vitronectin gene in astrocytic tumors. *J Cell Sci, 108 (Pt 3)*, 947-956.

Gudzenko, T., & Franz, C. M. (2015). Studying early stages of fibronectin fibrillogenesis in living cells by atomic force microscopy. *Mol Biol Cell, 26*(18), 3190-3204. doi:10.1091/mbc.E15-06-0421

Hodivala-Dilke, K. M., McHugh, K. P., Tsakiris, D. A., Rayburn, H., Crowley, D., Ullman-Culleré, M., . . . Hynes, R. O. (1999). Beta3-integrin-deficient mice are a model for Glanzmann thrombasthenia showing placental defects and reduced survival. *J Clin Invest, 103*(2), 229-238. doi:10.1172/JCI5487

Humphries, J. D., Byron, A., & Humphries, M. J. (2006). Integrin ligands at a glance. *J Cell Sci, 119*(Pt 19), 3901-3903. doi:10.1242/jcs.03098

Humphries, J. D., Wang, P., Streuli, C., Geiger, B., Humphries, M. J., & Ballestrem, C. (2007). Vinculin controls focal adhesion formation by direct interactions with talin and actin. *J Cell Biol, 179*(5), 1043-1057. doi:10.1083/jcb.200703036

Hytönen, V. P., & Wehrle-Haller, B. (2014). Protein conformation as a regulator of cell-matrix adhesion. *Phys Chem Chem Phys, 16*(14), 6342-6357. doi:10.1039/c3cp54884h

Jorgensen, W. L., & Madura, J. D. (1983). Quantum and statistical mechanical studies of liquids. 25. Solvation and conformation of methanol in water. *Journal of the American Chemical Society, 105*(6), 1407-1413. doi:10.1021/ja00344a001

Kandow, C. E., Georges, P. C., Janmey, P. A., & Beningo, K. A. (2007). Polyacrylamide hydrogels for cell mechanics: steps toward optimization and alternative uses. *Methods Cell Biol, 83*, 29-46. doi:10.1016/s0091-679x(07)83002-0

Kaukonen, R., Jacquemet, G., Hamidi, H., & Ivaska, J. (2017). Cell-derived matrices for studying cell proliferation and directional migration in a complex 3D microenvironment. *Nat Protoc, 12*(11), 2376-2390. doi:10.1038/nprot.2017.107

Keasey, M. P., Jia, C., Pimentel, L. F., Sante, R. R., Lovins, C., & Hagg, T. (2018). Blood vitronectin is a major activator of LIF and IL-6 in the brain through integrin-FAK and uPAR signaling. *J Cell Sci, 131*(3). doi:10.1242/jcs.202580

Kronenberg, N. M., Liehm, P., Steude, A., Knipper, J. A., Borger, J. G., Scarcelli, G., . . . Gather, M. C. (2017). Long-term imaging of cellular forces with high precision by elastic resonator interference stress microscopy. *Nat Cell Biol, 19*(7), 864-872. doi:10.1038/ncb3561

Kuo, J. C., Han, X., Hsiao, C. T., Yates, J. R., 3rd, & Waterman, C. M. (2011). Analysis of the myosin-II-responsive focal adhesion proteome reveals a role for beta-Pix in negative regulation of focal adhesion maturation. *Nat Cell Biol, 13*(4), 383-393. doi:10.1038/ncb2216

Langhe, R. P., Gudzenko, T., Bachmann, M., Becker, S. F., Gonnermann, C., Winter, C., . . . Kashef, J. (2016). Cadherin-11 localizes to focal adhesions and promotes cell-substrate adhesion. *Nat Commun, 7*, 10909. doi:10.1038/ncomms10909

Lehnert, D., Wehrle-Haller, B., David, C., Weiland, U., Ballestrem, C., Imhof, B. A., & Bastmeyer, M. (2004). Cell behaviour on micropatterned substrata: limits of extracellular matrix geometry for spreading and adhesion. *J Cell Sci, 117*(Pt 1), 41-52. doi:117/1/41 [pii]

10.1242/jcs.00836

Li, J., Su, Y., Xia, W., Qin, Y., Humphries, M. J., Vestweber, D., . . . Springer, T. A. (2017). Conformational equilibria and intrinsic affinities define integrin activation. E*mbo j, 36(*5), 629-645. doi:10.15252/embj.201695803

Lindorff-Larsen, K., Piana, S., Palmo, K., Maragakis, P., Klepeis, J. L., Dror, R. O., & Shaw, D. E. (2010). Improved side-chain torsion potentials for the Amber ff99SB protein force field. P*roteins, 78(*8), 1950-1958. doi:10.1002/prot.22711

Luo, B. H., Springer, T. A., & Takagi, J. (2003). Stabilizing the open conformation of the integrin headpiece with a glycan wedge increases affinity for ligand. P*roc Natl Acad Sci U S A, 100(*5), 2403-2408. doi:10.1073/pnas.0438060100

Mas-Moruno, C., Rechenmacher, F., & Kessler, H. (2010). Cilengitide: the first anti-angiogenic small molecule drug candidate design, synthesis and clinical evaluation. A*nticancer Agents Med Chem, 10(*10), 753-768.

Mierke, C. T., Kollmannsberger, P., Zitterbart, D. P., Diez, G., Koch, T. M., Marg, S., . . . Fabry, B. (2010). Vinculin facilitates cell invasion into three-dimensional collagen matrices. J *Biol Chem, 285(*17), 13121-13130. doi:10.1074/jbc.M109.087171

Miyazaki, N., Iwasaki, K., & Takagi, J. (2018). A systematic survey of conformational states in beta1 and beta4 integrins using negative-stain electron microscopy. J *Cell Sci, 131(*10). doi:10.1242/jcs.216754

Pankov, R., & Yamada, K. M. (2002). Fibronectin at a glance. J *Cell Sci, 115(*Pt 20), 3861-3863.

Pierschbacher, M. D., & Ruoslahti, E. (1987). Influence of stereochemistry of the sequence Arg-Gly-Asp-Xaa on binding specificity in cell adhesion. J *Biol Chem, 262(*36), 17294-17298.

Pinon, P., Pärssinen, J., Vazquez, P., Bachmann, M., Rahikainen, R., Jacquier, M. C., . . . Wehrle-Haller, B. (2014). Talin-bound NPLY motif recruits integrin-signaling adapters to regulate cell spreading and mechanosensing. J *Cell Biol, 205(*2), 265-281. doi:10.1083/jcb.201308136

Plotnikov, S. V., Sabass, B., Schwarz, U. S., & Waterman, C. M. (2014). High-resolution traction force microscopy. M*ethods Cell Biol, 123,* 367-394. doi:10.1016/b978-0-12-420138-5.00020-3

Preissner, K. T., & Reuning, U. (2011). Vitronectin in vascular context: facets of a multitalented matricellular protein. S*emin Thromb Hemost, 37(*4), 408-424. doi:10.1055/s-0031-1276590

Puklin-Faucher, E., Gao, M., Schulten, K., & Vogel, V. (2006). How the headpiece hinge angle is opened: New insights into the dynamics of integrin activation. J *Cell Biol, 175(*2), 349-360. doi:10.1083/jcb.200602071

Pytela, R., Pierschbacher, M. D., & Ruoslahti, E. (1985). A 125/115-kDa cell surface receptor specific for vitronectin interacts with the arginine-glycine-aspartic acid adhesion sequence derived from fibronectin. P*roc Natl Acad Sci U S A, 82(*17), 5766-5770.

Rahikainen, R., von Essen, M., Schaefer, M., Qi, L., Azizi, L., Kelly, C., . . . Hytonen, V. P. (2017). Mechanical stability of talin rod controls cell migration and substrate sensing. S*ci Rep, 7(*1), 3571. doi:10.1038/s41598-017-03335-2

Richter, B., Hahn, V., Bertels, S., Claus, T. K., Wegener, M., Delaittre, G., . . . Bastmeyer, M. (2017). Guiding Cell Attachment in 3D Microscaffolds Selectively Functionalized with Two Distinct Adhesion Proteins. A*dv Mater, 29(*5). doi:10.1002/adma.201604342

Roca-Cusachs, P., Gauthier, N. C., Del Rio, A., & Sheetz, M. P. (2009). Clustering of alpha(5)beta(1) integrins determines adhesion strength whereas alpha(v)beta(3) and talin enable mechanotransduction. P*roc Natl Acad Sci U S A, 106(*38), 16245-16250. doi:10.1073/pnas.0902818106

Saltel, F., Mortier, E., Hytönen, V. P., Jacquier, M. C., Zimmermann, P., Vogel, V., . . . Wehrle-Haller, B. (2009). New PI(4,5)P2- and membrane proximal integrin-binding motifs in the talin head control beta3-integrin clustering. J *Cell Biol, 187(*5), 715-731. doi:10.1083/jcb.200908134

Schiller, H. B., Friedel, C. C., Boulegue, C., & Fässler, R. (2011). Quantitative proteomics of the integrin adhesome show a myosin II-dependent recruitment of LIM domain proteins. E*MBO Rep, 12(*3), 259-266. doi:10.1038/embor.2011.5

Schiller, H. B., Hermann, M. R., Polleux, J., Vignaud, T., Zanivan, S., Friedel, C. C., . . . Fässler, R. (2013). β1- and αv-class integrins cooperate to regulate myosin II during rigidity sensing of fibronectin-based microenvironments. N*at Cell Biol, 15(*6), 625-636. doi:10.1038/ncb2747

Schindelin, J., Rueden, C. T., Hiner, M. C., & Eliceiri, K. W. (2015). The ImageJ ecosystem: An open platform for biomedical image analysis. M*ol Reprod Dev, 82(*7-8), 518-529. doi:10.1002/mrd.22489

Soto-Ribeiro, M., Kastberger, B., Bachmann, M., Azizi, L., Fouad, K., Jacquier, M. C., . . . Wehrle-Haller, B. (2019). β1D integrin splice variant stabilizes integrin dynamics and reduces integrin signaling by limiting paxillin recruitment. J *Cell Sci, 132(*8). doi:10.1242/jcs.224493

Sousa da Silva, A. W., & Vranken, W. F. (2012). ACPYPE - AnteChamber PYthon Parser interfacE. B*MC Res Notes, 5,* 367. doi:10.1186/1756-0500-5-367

Takagi, J., Petre, B. M., Walz, T., & Springer, T. A. (2002). Global conformational rearrangements in integrin extracellular domains in outside-in and inside-out signaling. C*ell, 110(*5), 599-511.

Takahashi, S., Leiss, M., Moser, M., Ohashi, T., Kitao, T., Heckmann, D., . . . Fässler, R. (2007). The RGD motif in fibronectin is essential for development but dispensable for fibril assembly. J *Cell Biol, 178(*1), 167-178. doi:10.1083/jcb.200703021

Thievessen, I., Thompson, P. M., Berlemont, S., Plevock, K. M., Plotnikov, S. V., Zemljic-Harpf, A., . . . Waterman, C. M. (2013). Vinculin-actin interaction couples actin retrograde flow to focal adhesions, but is dispensable for focal adhesion growth. J *Cell Biol, 202(*1), 163-177. doi:10.1083/jcb.201303129

van der Flier, A., Badu-Nkansah, K., Whittaker, C. A., Crowley, D., Bronson, R. T., Lacy-Hulbert, A., & Hynes, R. O. (2010). Endothelial alpha5 and alphav integrins cooperate in remodeling of the vasculature during development. D*evelopment, 137(*14), 2439-2449. doi:10.1242/dev.049551

Van Der Spoel, D., Lindahl, E., Hess, B., Groenhof, G., Mark, A. E., & Berendsen, H. J. (2005). GROMACS: fast, flexible, and free. J *Comput Chem, 26(*16), 1701-1718. doi:10.1002/jcc.20291

Wang, S., Wu, C., Zhang, Y., Zhong, Q., Sun, H., Cao, W., . . . Chen, J. (2018). Integrin alpha4beta7 switches its ligand specificity via distinct conformer-specific activation. J *Cell Biol, 217(*8), 2799-2812. doi:10.1083/jcb.201710022

Wehrle-Haller, B. (2007). Analysis of integrin dynamics by fluorescence recovery after photobleaching. M*ethods Mol Biol, 370,* 173-202. doi:10.1007/978-1-59745-353-0_13

Wennerberg, K., Lohikangas, L., Gullberg, D., Pfaff, M., Johansson, S., & Fassler, R. (1996). Beta 1 integrin-dependent and -independent polymerization of fibronectin. J *Cell Biol, 132(*1-2), 227-238.

White, D. P., Caswell, P. T., & Norman, J. C. (2007). alpha v beta3 and alpha5beta1 integrin recycling pathways dictate downstream Rho kinase signaling to regulate persistent cell migration. J *Cell Biol, 177(*3), 515-525. doi:10.1083/jcb.200609004

Xiong, J. P., Stehle, T., Zhang, R., Joachimiak, A., Frech, M., Goodman, S. L., & Arnaout, M. A. (2002). Crystal structure of the extracellular segment of integrin alpha Vbeta3 in complex with an Arg-Gly-Asp ligand. S*cience, 296(*5565), 151-155. doi:10.1126/science.1069040

Yang, J. T., Bader, B. L., Kreidberg, J. A., Ullman-Culleré, M., Trevithick, J. E., & Hynes, R. O. (1999). Overlapping and independent functions of fibronectin receptor integrins in early mesodermal development. D*ev Biol, 215(*2), 264-277. doi:10.1006/dbio.1999.9451

Ye, F., Hu, G., Taylor, D., Ratnikov, B., Bobkov, A. A., McLean, M. A., . . . Ginsberg, M. H. (2010). Recreation of the terminal events in physiological integrin activation. J *Cell Biol, 188(*1), 157-173. doi:10.1083/jcb.200908045

Zhu, J., Luo, B. H., Xiao, T., Zhang, C., Nishida, N., & Springer, T. A. (2008). Structure of a complete integrin ectodomain in a physiologic resting state and activation and deactivation by applied forces. M*ol Cell, 32(*6), 849-861. doi:10.1016/j.molcel.2008.11.018

Zhu, J., & Springer, T. A. (2013). Complete integrin headpiece opening in eight steps. J *Cell Biol, 201(*7), 1053-1068. doi:10.1083/jcb.201212037

Figure 1

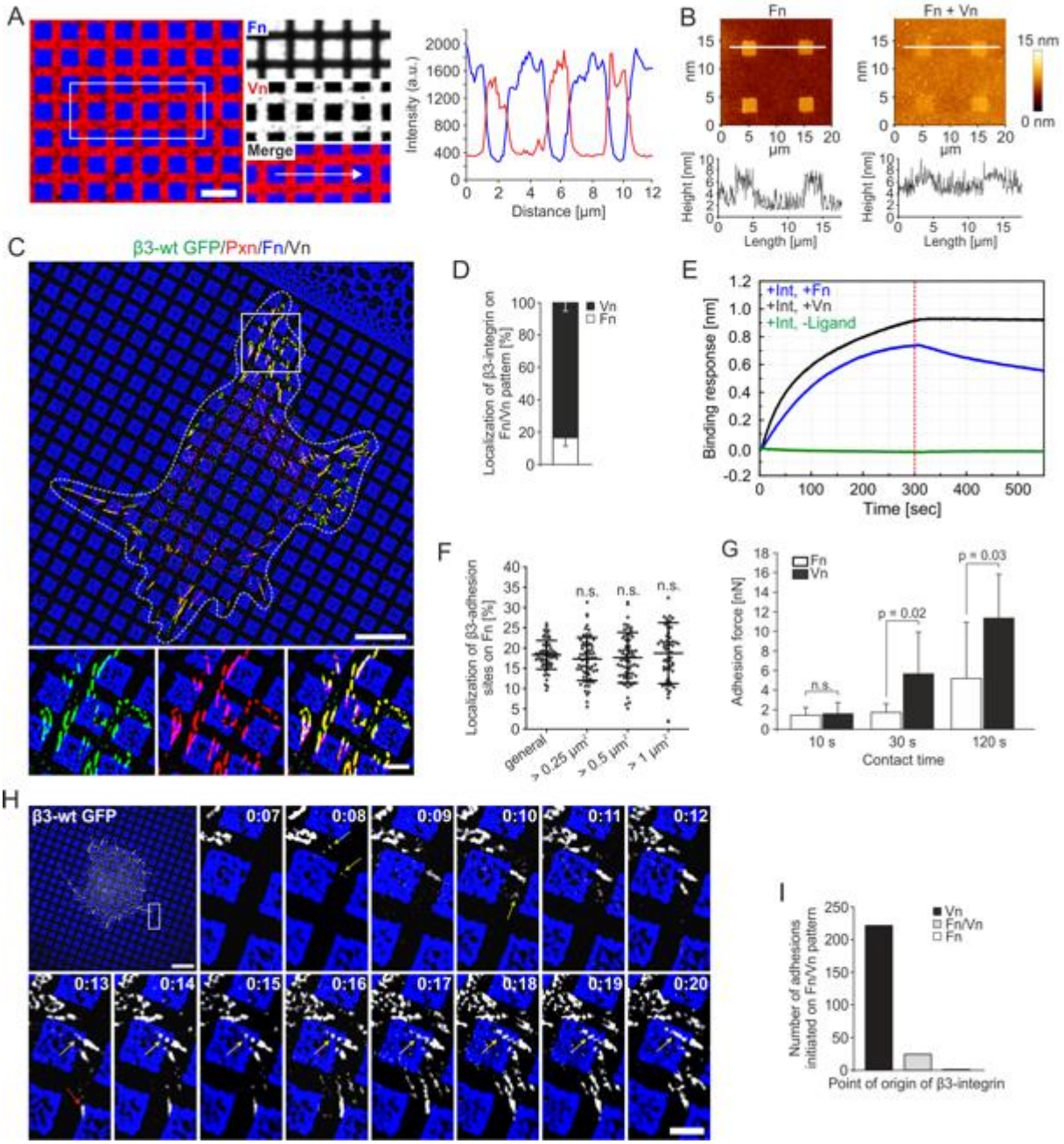
A
Fn
Vn
Merge
Intensity (a.u.)
Distance [µm]
B
Fn
Fn + Vn
15 nm
0 nm
nm
µm
Height [nm]
Length [µm]
C
β3-wt GFP/Pxn/Fn/Vn
D
Localization of β3-integrin on Fn/Vn pattern [%]
Vn
Fn
E
+Int, +Fn
+Int, +Vn
+Int, -Ligand
Binding response [nm]
Time [sec]
F
Localization of β3-adhesion sites on Fn [%]
n.s.
general
> 0.25 µm²
> 0.5 µm²
> 1 µm²
G
Fn
Vn
Adhesion force [nN]
p = 0.02
p = 0.03
10 s
30 s
120 s
Contact time
H
β3-wt GFP
0:07
0:08
0:09
0:10
0:11
0:12
0:13
0:14
0:15
0:16
0:17
0:18
0:19
0:20
I
Vn
Fn/Vn
Fn
Number of adhesions initiated on Fn/Vn pattern
Point of origin of β3-integrin

Figure 2

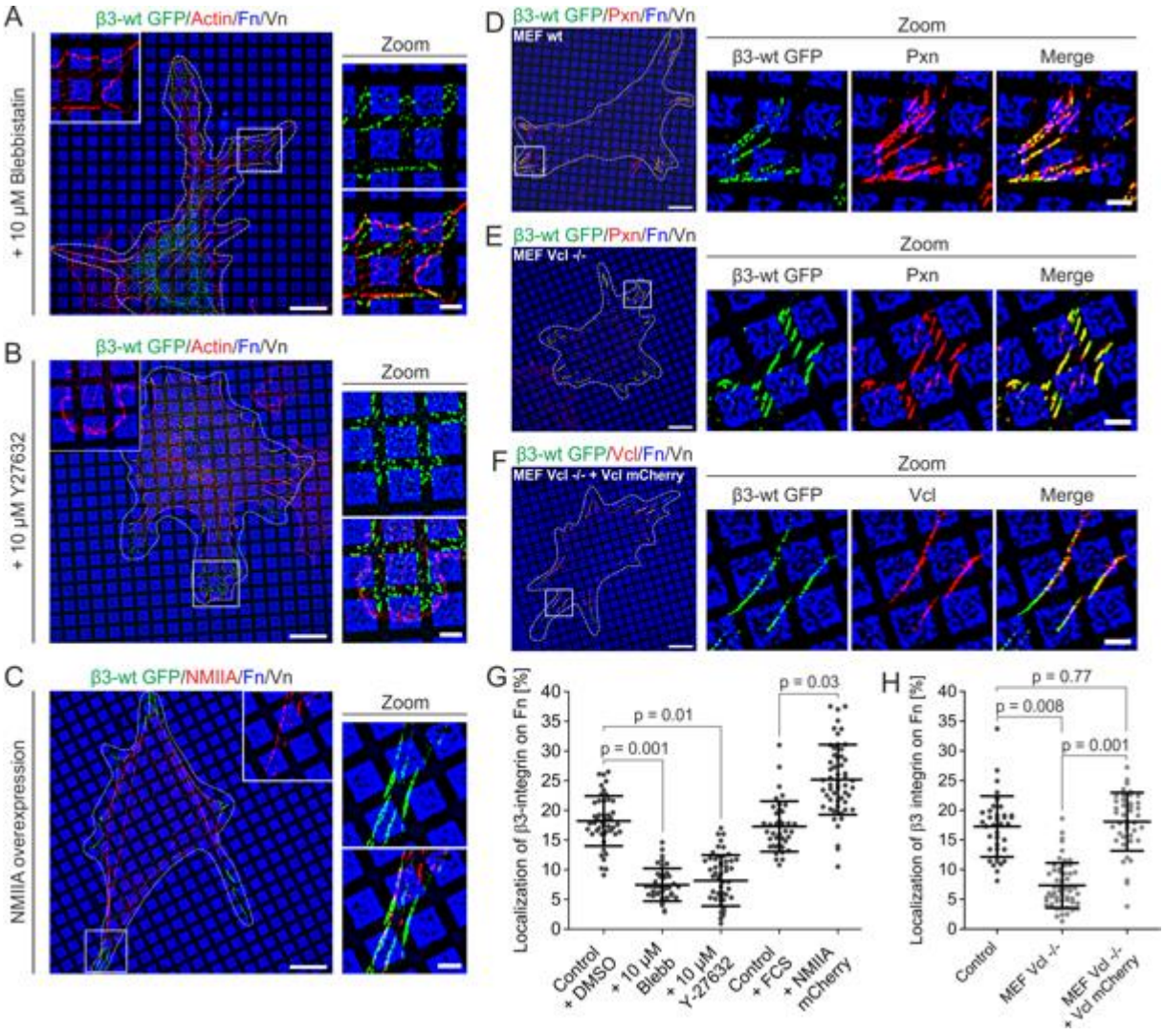
A
β3-wt GFP/Actin/Fn/Vn
+ 10 µM Blebbistatin
Zoom
B
β3-wt GFP/Actin/Fn/Vn
+ 10 µM Y27632
Zoom
C
β3-wt GFP/NMIIA/Fn/Vn
NMIIA overexpression
Zoom
D
β3-wt GFP/Pxn/Fn/Vn
MEF wt
Zoom
β3-wt GFP
Pxn
Merge
E
β3-wt GFP/Pxn/Fn/Vn
MEF Vcl -/-
Zoom
β3-wt GFP
Pxn
Merge
F
β3-wt GFP/Vcl/Fn/Vn
MEF Vcl -/- + Vcl mCherry
Zoom
β3-wt GFP
Vcl
Merge
G
Localization of β3-integrin on Fn [%]
p = 0.001
p = 0.01
p = 0.03
Control + DMSO
+ 10 µM Blebb
+ 10 µM Y-27632
Control + FCS
+ NMIIA mCherry
H
Localization of β3 integrin on Fn [%]
p = 0.008
p = 0.77
p = 0.001
Control
MEF Vcl -/-
MEF Vcl -/- + Vcl mCherry

Figure 3

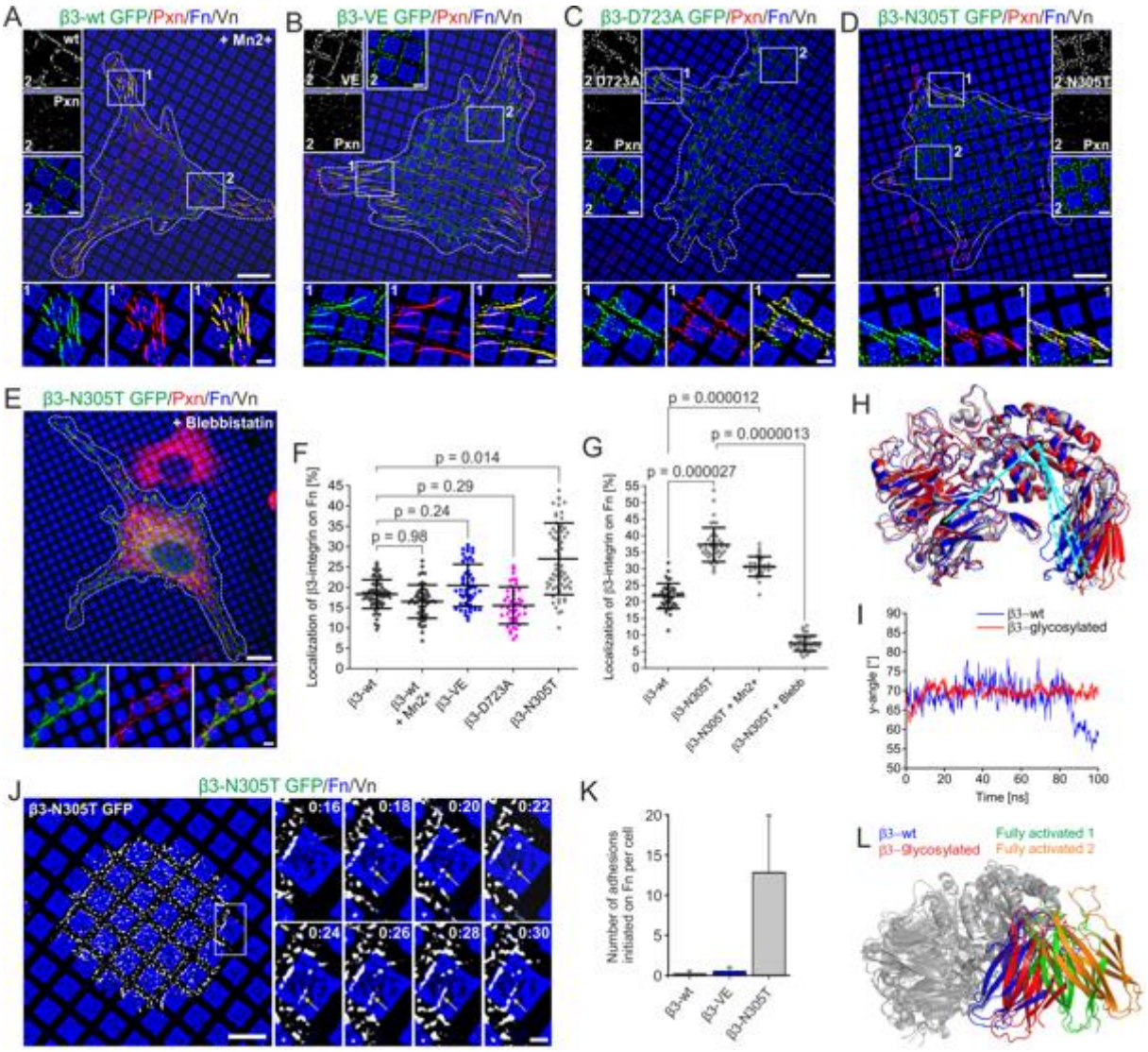
A
β3-wt GFP/Pxn/Fn/Vn
+ Mn2+
wt
Pxn
B
β3-VE GFP/Pxn/Fn/Vn
VE
Pxn
C
β3-D723A GFP/Pxn/Fn/Vn
D723A
Pxn
D
β3-N305T GFP/Pxn/Fn/Vn
N305T
Pxn
E
β3-N305T GFP/Pxn/Fn/Vn
+ Blebbistatin
F
Localization of β3-integrin on Fn [%]
p = 0.014
p = 0.29
p = 0.24
p = 0.98
β3-wt
β3-wt + Mn2+
β3-VE
β3-D723A
β3-N305T
G
Localization of β3-integrin on Fn [%]
p = 0.000012
p = 0.0000013
p = 0.000027
β3-wt
β3-N305T
β3-N305T + Mn2+
β3-N305T + Blebb
H
I
β3--wt
β3--glycosylated
γ-angle [°]
Time [ns]
J
β3-N305T GFP/Fn/Vn
β3-N305T GFP
0:16
0:18
0:20
0:22
0:24
0:26
0:28
0:30
K
Number of adhesions initiated on Fn per cell
β3-wt
β3-VE
β3-N305T
L
β3--wt
β3--Glycosylated
Fully activated 1
Fully activated 2

Figure 4

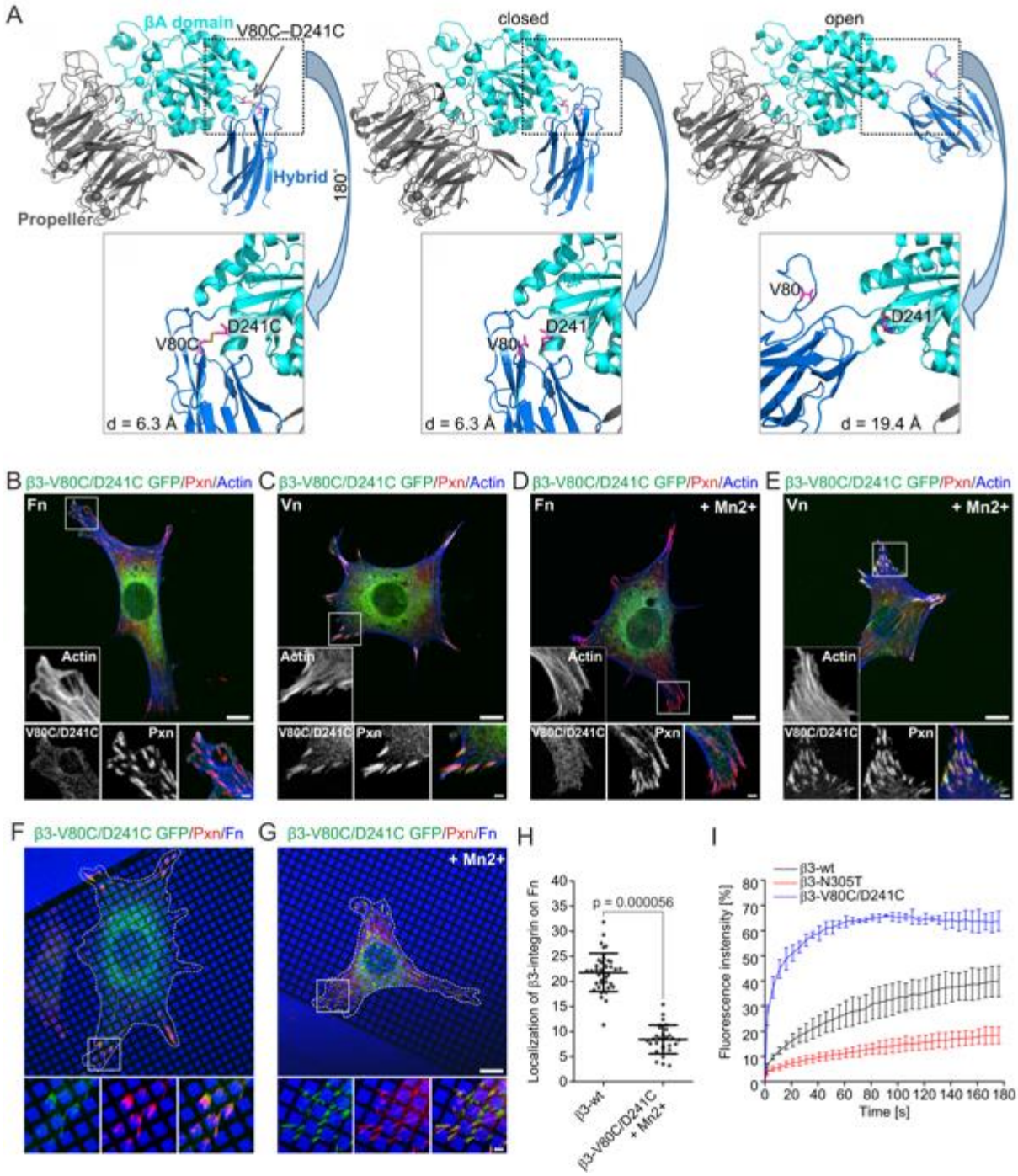
A
βA domain
V80C–D241C
Hybrid
180°
Propeller
closed
open
D241C
V80C
d = 6.3 Å
D241
V80
d = 6.3 Å
V80
D241
d = 19.4 Å
B β3-V80C/D241C GFP/Pxn/Actin
C β3-V80C/D241C GFP/Pxn/Actin
D β3-V80C/D241C GFP/Pxn/Actin
E β3-V80C/D241C GFP/Pxn/Actin
Fn
Vn
+ Mn2+
Actin
V80C/D241C
Pxn
F β3-V80C/D241C GFP/Pxn/Fn
G β3-V80C/D241C GFP/Pxn/Fn
+ Mn2+
H
Localization of β3-integrin on Fn
p = 0.000056
β3-wt
β3-V80C/D241C + Mn2+
I
β3-wt
β3-N305T
β3-V80C/D241C
Fluorescence instensity [%]
Time [s]

Figure 5

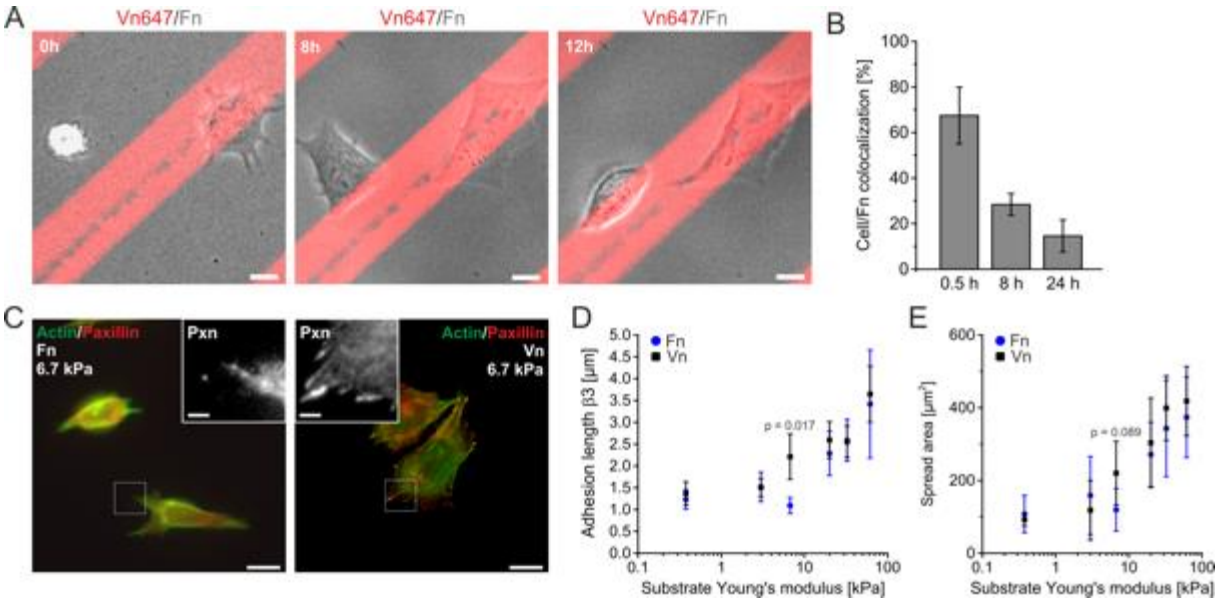
A
Vn647/Fn
0h
8h
12h
B
Cell/Fn colocalization [%]
0.5 h
8 h
24 h
C
Actin/Paxillin
Fn
6.7 kPa
Pxn
Vn
D
Fn
Vn
Adhesion length β3 [µm]
p = 0.017
Substrate Young's modulus [kPa]
E
Spread area [µm²]
p = 0.089

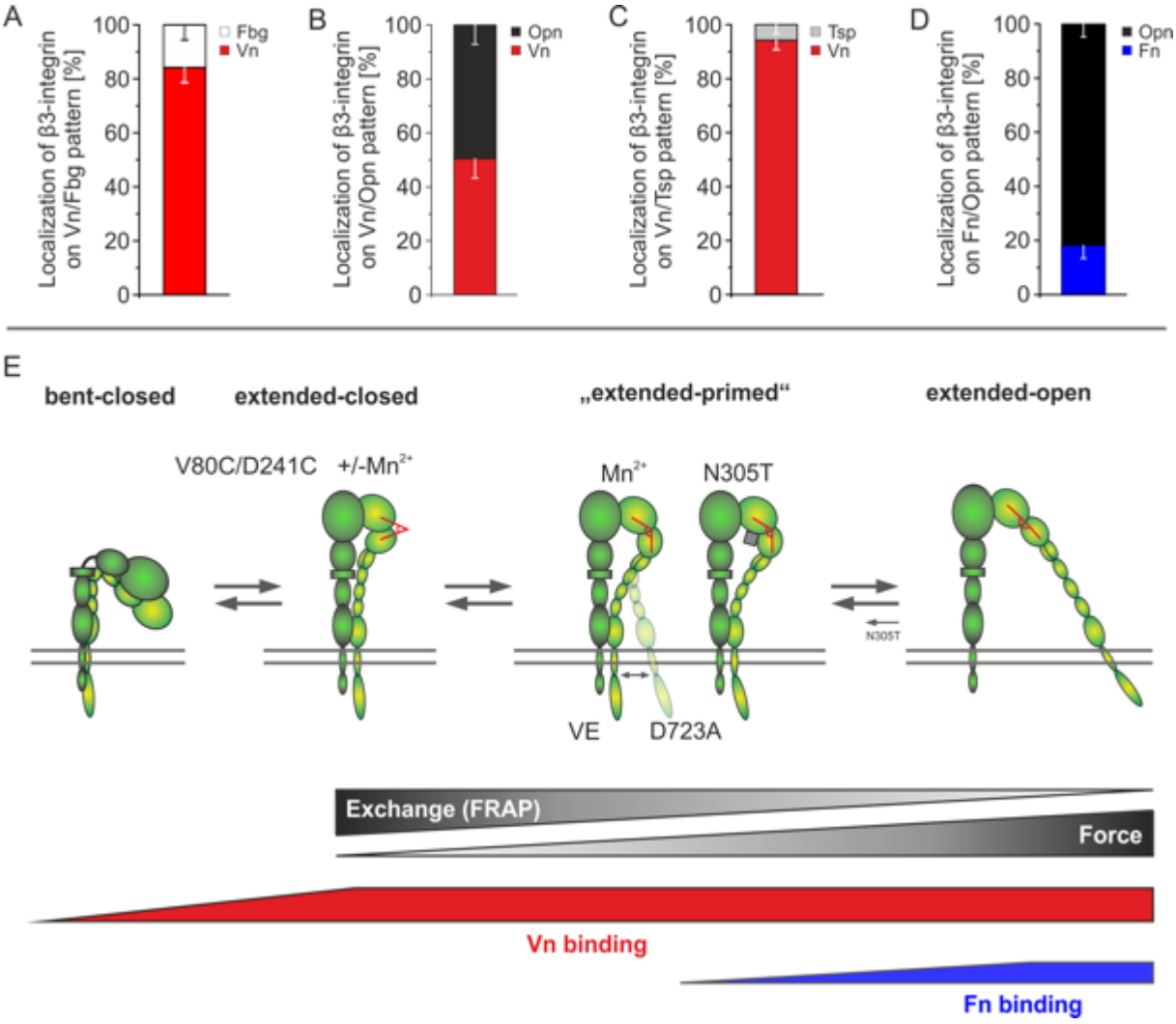
A
Localization of β3-integrin on Vn/Fbg pattern [%]
100
80
60
40
20
0
Fbg
Vn
B
Localization of β3-integrin on Vn/Opn pattern [%]
Opn
Vn
C
Localization of β3-integrin on Vn/Tsp pattern [%]
Tsp
Vn
D
Localization of β3-integrin on Fn/Opn pattern [%]
Opn
Fn
E
bent-closed
extended-closed
„extended-primed“
extended-open
V80C/D241C
+/-Mn2+
Mn2+
N305T
N305T
VE
D723A
Exchange (FRAP)
Force
Vn binding
Fn binding

SupFig 1

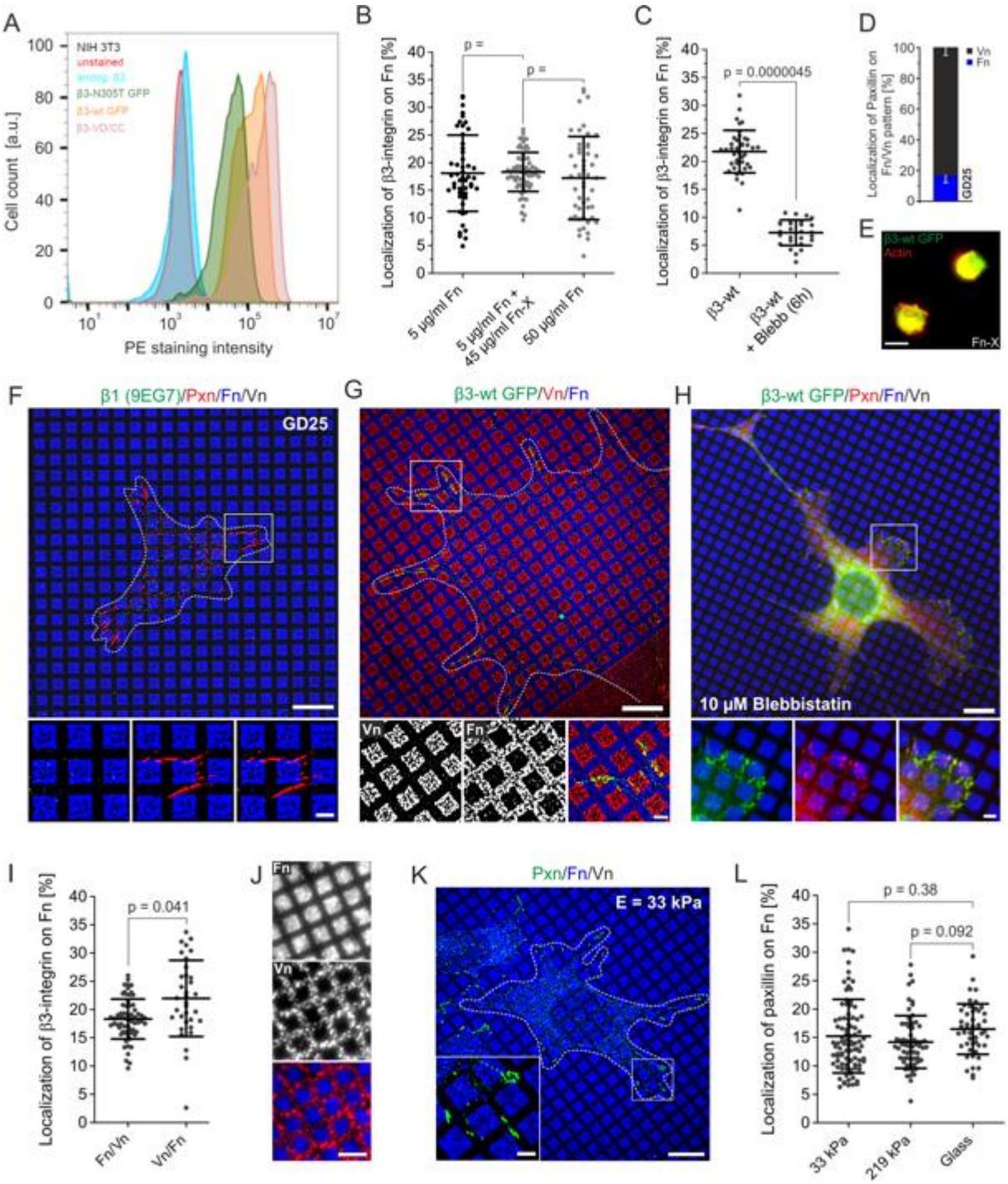
A
NIH 3T3
unstained
β3-N305T GFP
β3-wt GFP
β3-VDVCC
Cell count [a.u.]
PE staining intensity
B
Localization of β3-integrin on Fn [%]
p =
p =
5 µg/ml Fn
5 µg/ml Fn + 45 µg/ml Fn-X
50 µg/ml Fn
C
Localization of β3-integrin on Fn [%]
p = 0.0000045
β3-wt
β3-wt + Blebb (6h)
D
Localization of Paxillin on Fn/Vn pattern [%]
Vn
Fn
GD25
E
β3-wt GFP
Actin
Fn-X
F
β1 (9EG7)/Pxn/Fn/Vn
GD25
G
β3-wt GFP/Vn/Fn
Vn
Fn
H
β3-wt GFP/Pxn/Fn/Vn
10 µM Blebbistatin
I
Localization of β3-integrin on Fn [%]
p = 0.041
Fn/Vn
Vn/Fn
J
Fn
Vn
K
Pxn/Fn/Vn
E = 33 kPa
L
Localization of paxillin on Fn [%]
p = 0.38
p = 0.092
33 kPa
219 kPa
Glass

SupFig 2

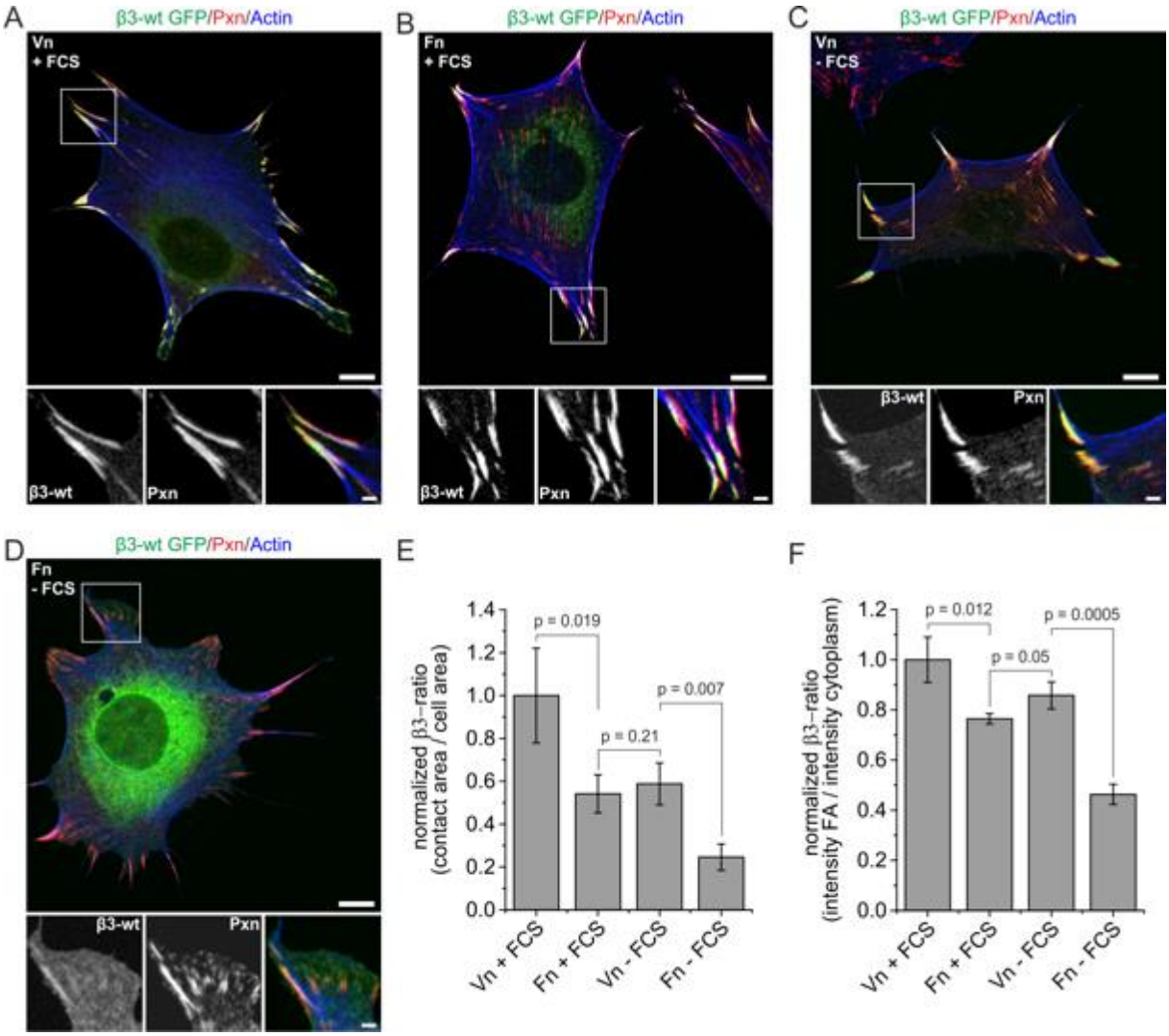
A
β3-wt GFP/Pxn/Actin
Vn
+ FCS
β3-wt
Pxn
B
β3-wt GFP/Pxn/Actin
Fn
+ FCS
β3-wt
Pxn
C
β3-wt GFP/Pxn/Actin
Vn
- FCS
β3-wt
Pxn
D
β3-wt GFP/Pxn/Actin
Fn
- FCS
β3-wt
Pxn
E
normalized β3-ratio
(contact area / cell area)
p = 0.019
p = 0.21
p = 0.007
Vn + FCS
Fn + FCS
Vn - FCS
Fn - FCS
F
normalized β3-ratio
(intensity FA / intensity cytoplasm)
p = 0.012
p = 0.05
p = 0.0005
Vn + FCS
Fn + FCS
Vn - FCS
Fn - FCS

SupFig 3

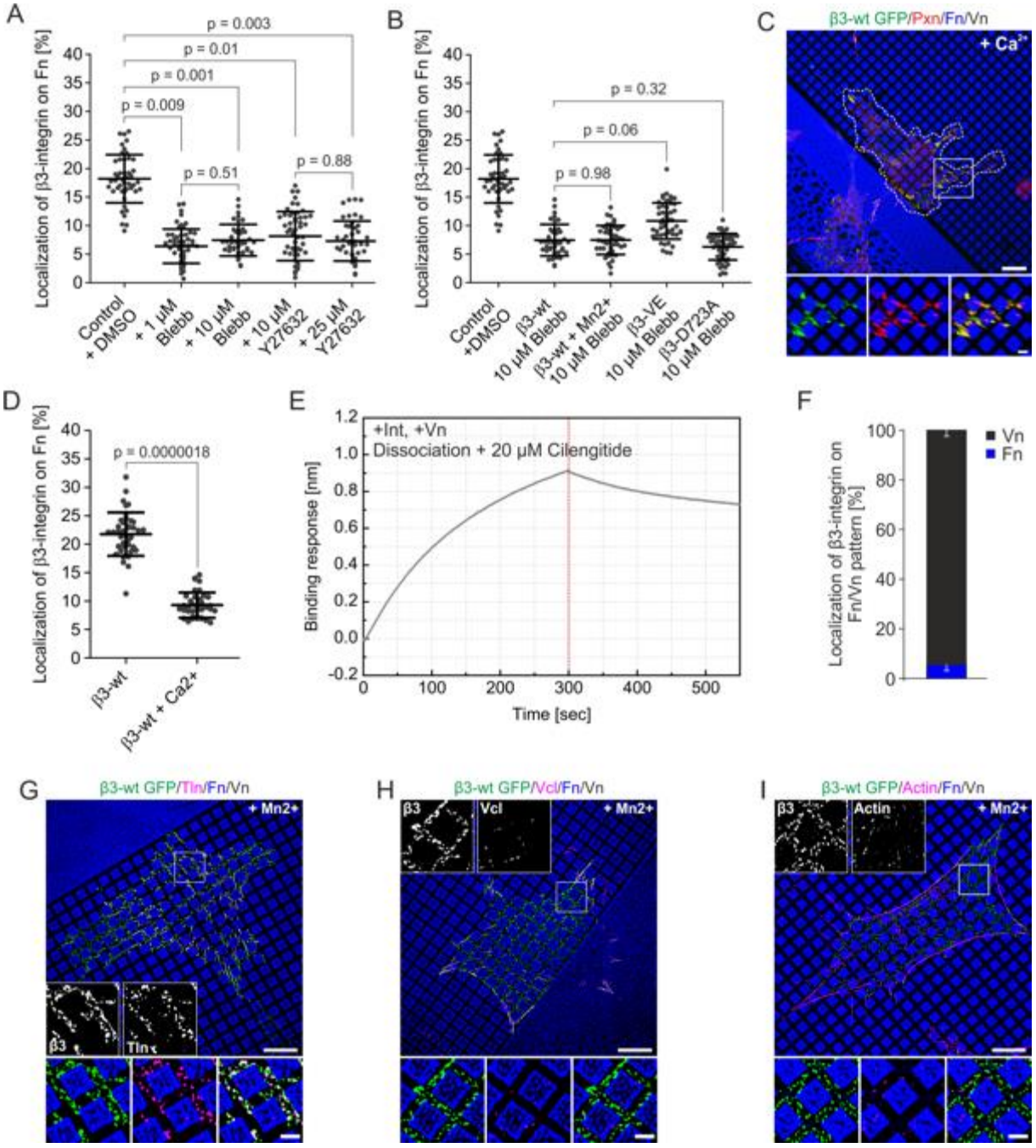
A
Localization of β3-integrin on Fn [%]
p = 0.003
p = 0.01
p = 0.001
p = 0.009
p = 0.51
p = 0.88
Control + DMSO
+ 1 µM Blebb
+ 10 µM Blebb
+ 10 µM Y27632
+ 25 µM Y27632
B
Localization of β3-integrin on Fn [%]
p = 0.32
p = 0.06
p = 0.98
Control +DMSO
β3-wt 10 µM Blebb
β3-wt + Mn2+ 10 µM Blebb
β3-VE 10 µM Blebb
β3-D723A 10 µM Blebb
C
β3-wt GFP/Pxn/Fn/Vn
+ Ca2+
D
Localization of β3-integrin on Fn [%]
p = 0.0000018
β3-wt
β3-wt + Ca2+
E
+Int, +Vn
Dissociation + 20 µM Cilengitide
Binding response [nm]
Time [sec]
F
Localization of β3-integrin on Fn/Vn pattern [%]
Vn
Fn
G
β3-wt GFP/Tln/Fn/Vn
+ Mn2+
β3
Tln
H
β3-wt GFP/Vcl/Fn/Vn
β3
Vcl
+ Mn2+
I
β3-wt GFP/Actin/Fn/Vn
β3
Actin
+ Mn2+

SupFig 4

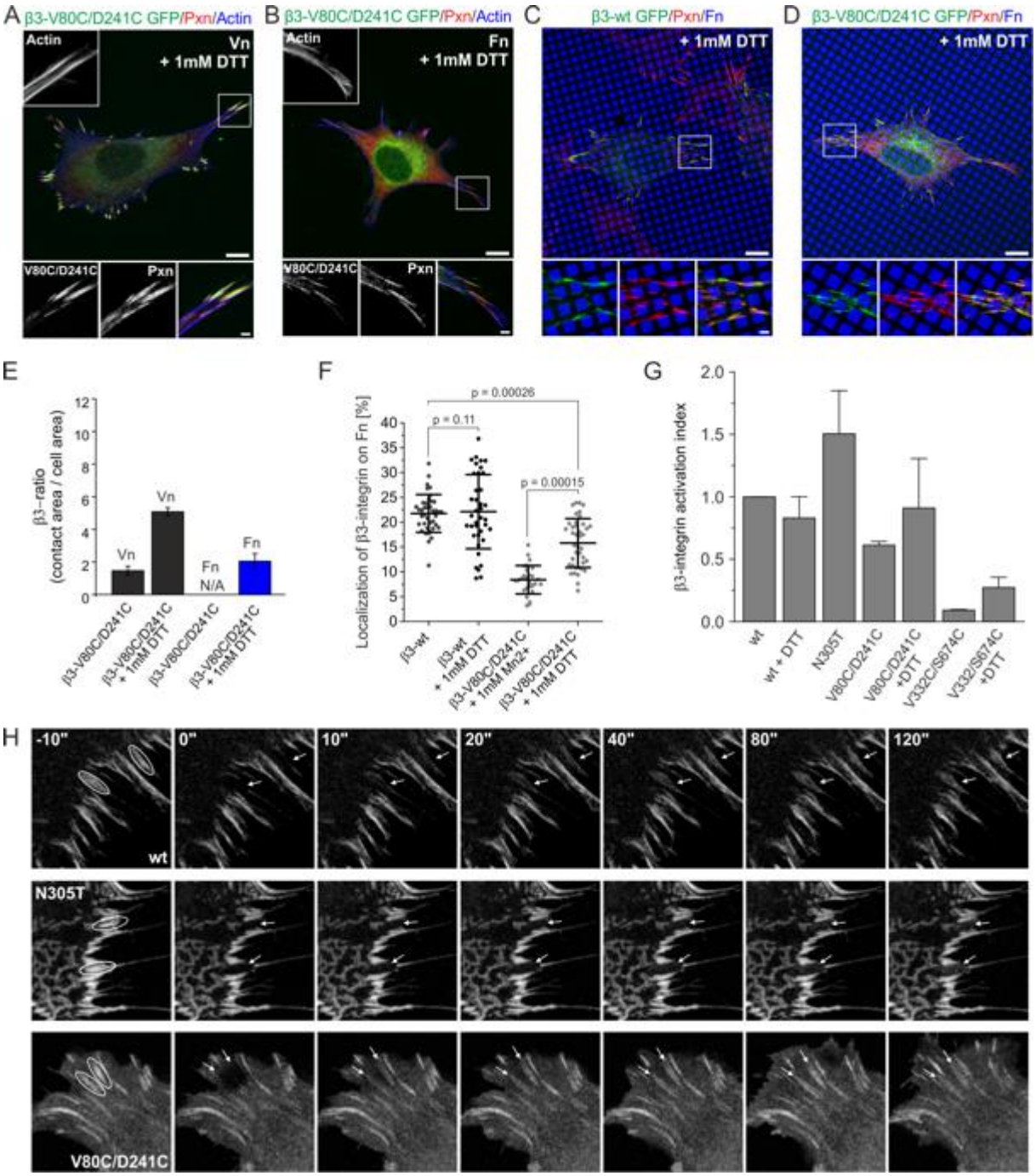
A β3-V80C/D241C GFP/Pxn/Actin
Actin
Vn
+ 1mM DTT
V80C/D241C
Pxn
B β3-V80C/D241C GFP/Pxn/Actin
Actin
Fn
+ 1mM DTT
V80C/D241C
Pxn
C β3-wt GFP/Pxn/Fn
+ 1mM DTT
D β3-V80C/D241C GFP/Pxn/Fn
+ 1mM DTT
E
β3-ratio (contact area / cell area)
Vn
Vn
Fn N/A
Fn
β3-V80C/D241C
β3-V80C/D241C + 1mM DTT
β3-V80C/D241C
β3-V80C/D241C + 1mM DTT
F
Localization of β3-integrin on Fn [%]
p = 0.00026
p = 0.11
p = 0.00015
β3-wt
β3-wt + 1mM DTT
β3-V80C/D241C + 1mM Mn2+
β3-V80C/D241C + 1mM DTT
G
β3-integrin activation index
wt
wt + DTT
N305T
V80C/D241C
V80C/D241C +DTT
V332C/S674C
V332/S674C +DTT
H
-10"
0"
10"
20"
40"
80"
120"
wt
N305T
V80C/D241C

SupFig 5

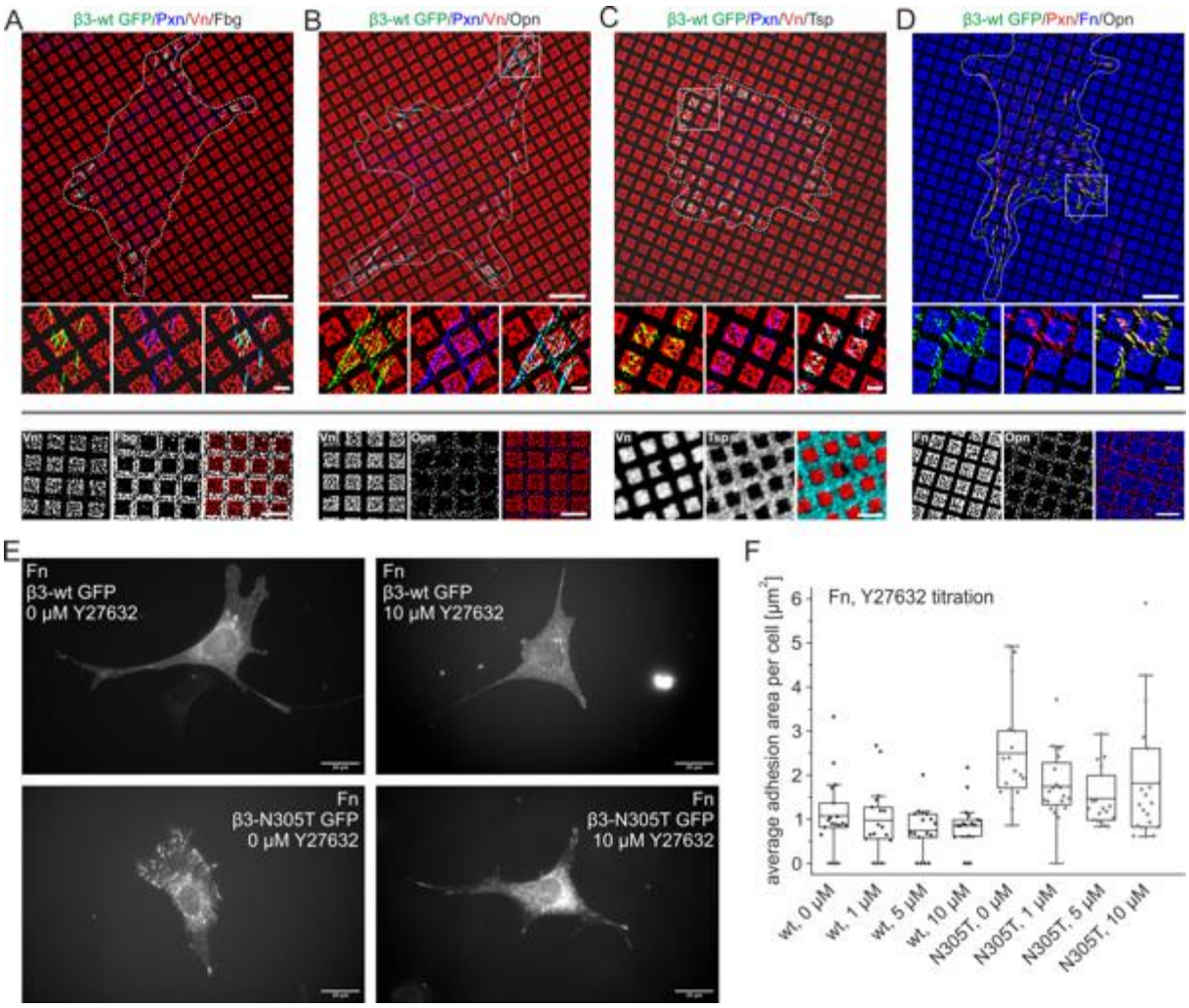
A
β3-wt GFP/Pxn/Vn/Fbg
B
β3-wt GFP/Pxn/Vn/Opn
C
β3-wt GFP/Pxn/Vn/Tsp
D
β3-wt GFP/Pxn/Fn/Opn
E
Fn
β3-wt GFP
0 μM Y27632
Fn
β3-wt GFP
10 μM Y27632
Fn
β3-N305T GFP
0 μM Y27632
Fn
β3-N305T GFP
10 μM Y27632
F
Fn, Y27632 titration
average adhesion area per cell [μm²]
0
1
2
3
4
5
6
wt, 0 μM
wt, 1 μM
wt, 5 μM
wt, 10 μM
N305T, 0 μM
N305T, 1 μM
N305T, 5 μM
N305T, 10 μM